Intestinal intraepithelial lymphocyte migration and tissue homeostasis are dictated by Gα13

Zachary M. Earley[1], Anshul Rao[1], Konrad Knöpper[1], Fanglue Peng[1], Longhui Qiu[2], Norihide Jo[1], Wioletta Lisicka[3], Hanna Taglinao[1,5], Jinping An[1], Ying Xu[1], Li V. Yang[4], Dan Liu[1,6], Mark R. Looney[2], Jason G. Cyster[1,*]

[1]Howard Hughes Medical Institute and Department of Microbiology and Immunology, University of California San Francisco, San Francisco, CA 94143, USA

[2]Department of Medicine and Department of Laboratory Medicine, University of California San Francisco, San Francisco, CA 94143, USA

[3]Department of Medicine, University of Chicago, Chicago, IL, USA

[4]Division of Hematology/Oncology, Department of Internal Medicine, Brody School of Medicine, East Carolina University, Greenville, NC, USA

[5]Current address: Department of Immunology, University of Washington, Seattle, WA, USA

[6]Current address: Westlake Laboratory of Life Sciences and Biomedicine, Westlake University School of Medicine, Hangzhou, China

*Lead Contact: jason.cyster@ucsf.edu

SUMMARY

The intestinal barrier harbors numerous intraepithelial lymphocytes (IEL) that promote tissue integrity and whose dysfunction contributes to disease. The signals regulating IEL dynamics are incompletely understood. Here we show that deficiency in heterotrimeric G-protein subunit Gα13 or effector Arhgef1 causes a loss of CD8αα and CD8αβ IEL. Following Gα13 ablation, IEL reduce migration speed prior to undergoing cell death. Induction of CD8αβ IEL by *Listeria monocytogenes* is intact but the cells fail to distribute along the villi and quickly die. TGFβ gain-of-function rescues Arhgef1-deficient CD8αβ cell numbers. CRISPR screening identifies a role for Gα13-coupled GPR132 in IEL homeostasis. T cell Gα13-deficient mice suffer more severe colitis and colorectal tumor growth. In summary, we identify Gα13 as an essential signaling node in αβ and γδ CD8 IEL and we propose Gα13-guided IEL positioning in the villous niche is required for receipt of signals, including TGFβ, for their maturation, survival and function.

INTRODUCTION

Intestinal intraepithelial lymphocytes (IELs) play an essential role in maintaining the intestinal barrier and provide a first line of defense against pathogens and intestinal tumors. There are an estimated 20-50 million IEL in the mouse small intestine (McDonald et al., 2018). IELs include

CD8 and CD4 T cells, with CD8 cells being predominant. CD8 IELs are divided into so-called unconventional T cells that include CD8αα expressing γδT cells and αβT cells that are programmed in the thymus, and conventional CD8αβ αβT cells that include T resident memory (Trm) cells induced during mucosal immune responses (McDonald *et al.*, 2018). Both γδT IEL and αβT IEL are motile and survey the epithelium, contacting multiple epithelial cells per hour (Edelblum et al., 2012; Hoytema van Konijnenburg et al., 2017; Thompson et al., 2019). The mechanisms responsible for T cell recruitment to the intestine have been extensively studied, with CCR9 playing an important role responding to CCL25 that is selectively expressed by small intestinal epithelium. The integrin α4β7 functions in T cell access to the small and large intestine and αEβ7 (CD103) contributes to retention in the intestine (Dai et al., 2021; Habtezion et al., 2016; Johansson-Lindbom and Agace, 2007; McDonald *et al.*, 2018). However, the full constellation of factors determining T cell migration within and positioning along the villi are unclear.

While the different IEL subsets occupy a similar niche, they have both shared and distinct requirements for their maintenance. γδT IEL are strongly dependent and CD8αα IEL partially dependent on IL15 and IL15Rα (McDonald *et al.*, 2018). CD8αβ IEL are less dependent on this cytokine receptor system alone, though they are reduced in number when both IL15 and IL7 are deficient (Jarjour et al., 2025). The process of conventional CD8αβ T cells becoming intestinal IEL involves priming in mesenteric lymph nodes (MLN) where retinoic acid (RA) promotes α4β7 and CCR9 expression (Hammerschmidt et al., 2008; Johansson-Lindbom and Agace, 2007; Molenaar et al., 2009; Qiu et al., 2023; Svensson et al., 2008). Following arrival in the intestine, the cells are exposed to locally activated TGFβ leading to a TGFβ-induced gene expression program that includes CD103 (Borges da Silva et al., 2020; Konkel et al., 2011; Sheridan et al., 2014; Zhang and Bevan, 2013). Persistence of CD8αβ cells in the intestine beyond a few days requires TGFβR signaling. In the LCMV infection setting, the primed CD8 T cells first appear in the crypts and over subsequent days accumulate along the length of the villi, with cells near the tips having a more mature Trm gene expression profile (Reina-Campos et al., 2025).

While chemokine receptors that couple to Gαi-containing heterotrimeric G-proteins have well established roles in guiding immune cell distribution, there have been increasing examples of Gα13-coupled receptors influencing cell positioning and homeostasis within tissues (Laidlaw et al., 2019; Liu et al., 2022; Lu and Cyster, 2019; Sumida et al., 2017). A key downstream effector of Gα13 is Arhgef1, a guanidine nucleotide exchange factor (GEF) for Rho (Aittaleb et al., 2010; Siehler, 2009). Although Gα13 is closely related to Gα12, multiple studies have established non-redundant roles for these Gα-proteins. A diverse set of GPCRs can couple to Gα13 and in most immune cell studies, these receptors inhibit migration towards chemoattractants (Laidlaw *et al.*, 2019; Lu and Cyster, 2019; Sumida *et al.*, 2017; Takuwa et al., 2011). A notable exception to this paradigm has been GPR132 (G2A), a receptor that can be stimulated in vitro by exposure to several lipid mediators including lysophosphatidylcholine (LPC), where a promigratory response occurs (Kabarowski et al., 2001; Radu et al., 2004; Wang et al., 2005; Yang et al., 2005). So far, the impact on IEL of deficiency in one Gα13-coupled

migration-inhibitory receptor, GPR55, has been reported and found to cause a mild increase in γδT cells (Sumida *et al.*, 2017). Whether other Gα13 coupled receptors influence intestinal T cell function is unclear.

Here we sought to broadly test the importance of Gα13-coupled receptors in intestinal immune homeostasis by deleting Gα13 in all hematopoietic cells. High dimensional flow cytometry revealed a striking loss of intestinal T cells that encompassed γδ T cells, CD8αα and CD8αβ αβT cells and that was T cell intrinsic. Conditional deletion of Gα13 led to a progressive loss of IEL that was preceded by a reduction in motility and increased apoptosis. Using a *Listeria monocytogenes (Lm)*-OVA intestinal infection model, Gα13-pathway deficient OVA-specific OT1 T cells reached the intestine in near normal numbers but failed to accumulate in the Trm compartment and showed reduced Bcl2 and deficient induction of TGFβ-pathway genes. Over-expression of Bcl2 or activated TGFβ was sufficient to partially restore Gα13-pathway deficient IEL. GPR132 was identified as a Gα13-coupled receptor contributing to CD8αβ IEL homeostasis. Finally, the lack of IEL caused by Gα13-deficiency led to more severe dextran sodium sulfate (DSS)-indued colitis and less ability to control colorectally implanted tumor cells.

RESULTS

Gα13 is required for intestinal IEL T cell homeostasis.

To broadly examine the role of Gα13 in intestinal immune cell homeostasis, Gna13f/f mice that had been crossed with the pan-hematopoietic VavCre line (Gα13ΔVav) were studied. Flow cytometric analysis with a 35 color antibody panel revealed a striking reduction in the CD8 T cell subsets with minimal impact on CD4 T cells (Fig. 1A). Analysis of further mice using a focused panel for CD8 and CD4 αβ and γδ T cells revealed a ~100 fold deficiency in γδT and CD8αα αβT IEL and a ~10-fold deficiency in CD8αβ αβT IEL while CD4 αβT IEL were not significantly affected (Fig. 1B, C). Similar findings were made for the colon (Fig. 1D). Small intestinal lamina propria (LP) CD8 T cell subsets were also greatly reduced (Suppl. Fig. S1A). The marked deficiency in γδT IEL and CD8αβ IEL was confirmed in immunofluorescence microscopy of small intestinal tissue sections (Fig. 1E and Fig. S1B). γδT and CD8αβ T cell numbers in other non-lymphoid tissues (skin, liver, lung) and in spleen and lymph nodes (LNs) were not affected (Suppl. Fig. S1C, D). The number of thymic CD8αα IEL precursor cells (Konkel *et al.*, 2011) was unchanged (Suppl. Fig. S1E). Staining for surface phosphatidylserine, a marker of apoptosis, with Annexin V showed that most of the remaining γδT cells in Gα13ΔVav mice were Annexin V^+ (Fig. 1F and Suppl. Fig. S1F).

To test for a T cell intrinsic role of Gα13 in IEL homeostasis we reconstituted irradiated mice with a mixture of WT (CD45.1/2) and Gα13ΔVav or WT control (CD45.2) bone marrow (BM). Analysis of the mixed BM chimeras after 8 weeks of reconstitution showed a marked γδT, CD8αα αβT and CD8αβ αβT IEL deficiency, establishing the essential role of this Gα protein in CD8 IEL (Fig. 1G). Under these competitive conditions there was a reduction in Gα13-deficient CD4 IEL (Fig. 1G). Analysis of mice lacking the Gα13 effector, Arhgef1, showed a similar γδT

and CD8 αβT IEL deficiency (Suppl. Fig. S1G). Using the mixed BM chimera approach, a similarly severe IEL defect was observed for Arhgef1-deficient as for Gα13-deficient chimeras (Fig. 1H) providing evidence that Gα13 acts in IEL homeostasis through engagement of Arhgef1.

To further test the αβT cell intrinsic role of Gα13 we generated Gna13f/f CD4Cre mice. CD4Cre is expressed in CD4 CD8 double positive (DP) thymocytes and therefore targets CD8 and CD4 T cells but not γδT cells (Hu et al., 2023). These mice showed a marked deficiency in CD8αα and CD8αβ αβT IEL, while γδT IEL were unaffected (Fig. 1I). Many CD8αβ T cells in WT mice expressed IFNγ as expected (McDonald *et al.*, 2018) whereas few of the CD8αβ IEL remaining in Gα13ΔCD4 mice expressed IFNv (Suppl. Fig. S1H). Overall, these data establish a selective high dependence of intestinal CD8 IEL on Gα13- and Arhgef1-signaling.

Conditional Gα13 deletion from IEL leads to defective motility and cell loss

To gain insight into the temporal requirement for Gα13 by IEL we crossed Gna13f/f mice with TCRδ-CreERT2 and E8iCreERT2 mice to enable tamoxifen mediated deletion of the Gna13 gene in mature γδT cell and CD8 T cells, respectively. Based on prior evidence that the TCRδ-CreERT2 had low activity and deletion was enhanced in mice harboring two alleles (Zhang et al., 2015) we studied TCRδ-CreERT2 homozygous mice and we included an Ai6 Rosa26-LSL-zsGreen reporter to mark cells that had experienced Cre activity (Suppl. Fig. S2A). We used five consecutive doses of tamoxifen as in previous work with this mouse line (Zhang *et al.*, 2015). Three days following tamoxifen treatment, a time point when there had likely been only partial loss of Gα13, there had been little change in γδT IEL numbers (Fig. 2A). By 2 weeks there was a substantial loss of γδT IEL (Fig. 2A). The E8iCreERT2 is efficacious (Andrews et al., 2021), and we found strong induction of reporter (Ai14-tdTom) expression following three days of tamoxifen treatment (Suppl. Fig. S2B). Gα13-deleted CD8αα and CD8αβ αβT IEL decayed from the intestine over a 1 week period (Fig. 2B). E8iCre is also active in $CD8^+$ γδT cells, and γδT IEL decayed over 1 week after tamoxifen treatment (Suppl. Fig. S2C).

We next asked how Gα13-deficiency impacted IEL motility. In transwell assays T cells from lymphoid organs show very limited migration (<5%) in the absence of chemokine (Matloubian et al., 2004; Okada and Cyster, 2007). In agreement with earlier work (Sumida *et al.*, 2017) we found that γδT IEL and CD8αβ T IEL had high basal migration in the absence of chemokine (30-70%). This constitutive motility was strongly dependent on Gα13 (Fig. 2C, D). To test the impact of Gα13-deficiency on IEL migration in vivo, we used intravital 2-photon microscopy (Edelblum *et al.*, 2012; Hoytema van Konijnenburg *et al.*, 2017). Intravital imaging of Gα13ΔTCRδ Ai6-ZsGreen reporter mice at day 3 after tamoxifen treatment (Fig. 2E), when the reporter had been activated but Gα13 protein likely had minimally decayed, revealed track speeds (Fig. 2F) and migration dynamics (Fig. 2G, Movie S1) similar to previous reports (Edelblum *et al.*, 2012; Hoytema van Konijnenburg *et al.*, 2017; Hu et al., 2018). By day 7, when γδT cell numbers had not significantly declined, the track speed and migration behavior was not significantly changed (Fig. 2G and Movie S2). However, by day 10 the track speed had decreased and for the $reporter^+$ cells remaining at day 14 there was a striking reduction in migration with some cells

moving and then stopping in association with the epithelium for the remaining duration of the movie (Fig. 2G and Movie S3 and S4). The confinement ratio, measured as displacement/time, was significantly reduced at day 14 (Fig. 2H). In a second approach, to allow imaging of WT and Gα13-deficient IEL in the same tissue, irradiated TCRβδ-/- mice were reconstituted with Ai14-tdTomato control and Gα13ΔTCRδ Ai6-ZsGreen BM. After an ~8 week reconstitution period, mice were treated with tamoxifen and the intestine imaged at day 14 (Fig. 2I). Control γδT cells were highly motile while most Gα13-deficient γδT cells in the same tissue volume showed greater confinement or failed to move during the imaging period (Fig. 2J, K and Movie S5 and S6). Taken together, these findings provide evidence that Gα13 expression contributes to the intrinsic motility of IEL and is required for their epithelial patrolling behavior.

Gene expression profile of Gα13-deficient intestinal T cells

To gain insight into the impact of Gα13-deficiency on IEL gene expression we performed 10x scRNAseq on a pool of sorted TCRγδ+ and TCRαβ+ CD8α+ and CD4+ IEL from control and Gα13ΔVav mice. This analysis revealed a striking shift in the gene expression profile of the γδT and CD8αβ αβT IEL remaining in Gα13ΔVav mice (Fig. 3A and Suppl. Fig. 3 A,B). The CD8αα αβT IEL were not well represented due to their several fold lower frequency amongst CD8α+ TCRαβ+ IEL than CD8αβ+ cells (Fig. 1C). An increased fraction of both γδT and αβT IEL were proliferating, perhaps a consequence of the marked loss of these cell types leaving an open niche that over-stimulates the rare survivors. The CD4 T cells also showed altered gene expression (Fig. 3A) possibly due to the profound loss of $CD8^+$ IEL but perhaps also reflecting intrinsic changes as suggested by their reduced competitiveness in mixed BM chimeras (Fig. 1G). Dot plot analysis showed reduced integrin Itgae and Itga1 expression in γδT and CD8αβ T IEL and reduced expression of IEL-associated transcription factors Nr4a2, Nr4a3, Junb, and Fosb and of the Trm transcription factor Runx3. Notably, γδT cells had markedly reduced Bcl2 expression and there was increased expression of pro-cell death genes Zbp1, Casp3, Casp4, Bax and Fas (Fig. 3B). The Gα13-deficient cells also had higher expression of certain genes associated with naïve cells, including Klf2, S1pr1 and Ly6a, perhaps indicative of a less differentiated state and recent recruitment to the IEL compartment (Fig. 3B). Another notable feature of the Gα13-deficient γδT cells was a reduction in an IL15-induced signature (James et al., 2021) (Fig. 3C). A concern with this analysis was that the broad loss of Gα13 in hematopoietic cells may indirectly influence gene expression in the remaining IEL. We therefore performed RNAseq on CD8αβ IEL sorted from Gα13ΔCD4 mice. Among top genes that were more highly expressed in Gα13-deficient CD8αβ IEL were Tcf7, Klf2, S1pr1, Ccr7 and Sell, genes that are highly expressed in naïve T cells, again suggesting a less differentiated state (Fig. 3D). Genes that were less expressed in KO cells included effector program associated molecules such as Prdm1, Itga1, Gzma, the cytokine Ifng, IEL-associated transcription factors Egr2, Nr4a2, Nr4a3, Junb, and Fos, and survival promoting factors Il7r and Bcl2 (Fig. 3D, E). Pathway analysis highlighted impacts of Gα13-deficiency on chemotaxis/migration, TGFβ, STAT5 and NFkB signaling, mTORC signaling, and programmed cell death (Fig. 3E).

The reduced Bcl2 expression in γδT and CD8αβ αβT IEL (Fig. 3B, D, F) together with the evidence for increased apoptosis (Fig. 1F) led us to test the sufficiency of Bcl2 over-expression

to rescue Gα13-deficient IEL. BM from control (Gα13fl) or Gα13ΔVav mice was transduced with a retroviral construct encoding Bcl2 and a GFP reporter, or an empty vector encoding only GFP (EV-GFP). Analysis of the intestine of the chimeric mice 8 weeks after reconstitution showed Bcl2 was sufficient to greatly increase γδT and αβT IEL in Gα13ΔVav mice (Fig. 3G). These findings provide evidence that Gα13 function is required for intact signaling by several pathways and has effects that promote IEL survival.

G13 signaling controls the maturation and homeostasis of intestinal CD8αβ Trm

To test the role of G13-pathway signaling during intestinal CD8αβ IEL induction, we employed the *Lm*-OVA infection and OT1 TCR transgenic adoptive cell transfer model (Sheridan *et al.*, 2014). We used Arhgef1-deficient mice for these studies as the full genetic knockout avoided concerns about incomplete deletion of a floxed allele. Control or Arhgef1-deficient OT1 cells were transferred into mice that were gastrically infected with *Lm*-OVA (Fig. 4A). Analysis 8 days later revealed similar intestinal recruitment of control and Arhgef1-deficient cells (Fig. 4B). However, the number of Arhgef1-deficient cells began decaying relative to control by day 11 and they were 100-fold depleted by day 28 (Fig. 4B). Annexin V staining showed higher apoptosis amongst Arhgef1-deficient OT1 cells was already evident at day 8 (Fig. 4C). To determine the intestinal selectivity of the G13-pathway dependence, we infected WT and Gα13ΔCD4 mice with LCMV Armstrong and assessed LCMV-specific CD8 Trm in tissues using Gp33 tetramers at day 28. There was a marked reduction in tetramer+ IEL in the intestine but little reduction in skin, lung, spleen or LNs (Fig. 4D). The few remaining $GP33^{+}$ CD8αβ IELs in Gα13ΔCD4 mice at day 28 revealed a striking defect in tissue resident memory markers CD69 and CD103 (Fig. 4E). Although the appearance of similar numbers of OT1 CD8 T cells in the intestine at day 8 indicated intact homing, to further test this we activated WT and Gα13 KO CD8 T cells in vitro in the presence of RA and TGFβ to promote induction of CCR9 and α4β7 (Edele et al., 2008). The Gα13-deficient cells proliferated equivalently to WT cells, showed equivalent upregulation of CCR9 and α4β7, and intact transwell migration to CCL25 (Suppl. Fig. S4A, B). Adoptive transfer of these polyclonal gut tropic CD8 T cells to WT mice showed similar homing to the small intestine (Suppl. Fig. S4C). However, after 5 days, there were less Gα13-deficient compared to WT cells and by day 10 the loss of Gα13-deficient cells was marked (Suppl. Fig. S4C).

Based on RNAseq analysis of day 8 transferred OT1 cells, there was reduced TGFβ pathway activity in the absence of Arhgef1 (Fig. 4F). This included reduced expression of Itgae that encodes integrin αE, also called CD103, a known TGFβ-induced gene (Fig. 4G). Reduced CD103 expression was confirmed by flow cytometry and occurred at day 8 in the tissue, before notable cell loss was observed (Fig. 4G). Control OT1 cells upregulated CD103 from day 8 to day 11, however this process was impaired in the Arhgef1-deficient cells in accord with a defect in TGFβ signaling and thus Trm differentiation in the tissue (Fig. 4G). Immunofluorescence microscopy at day 8 showed control OT1 cells were distributed along the length of intestinal villi whereas Arhgef1-deficient OT1 were often more enriched near the villus base (crypt) (Fig. 4H and Suppl. Fig. S4D). This distribution is similar to findings for TGFβR-/- P14 CD8αβ T cells at the same time point (Reina-Campos *et al.*, 2025). To test whether the reduced TGFβ-induced genes contributed to the CD103 deficiency and impaired IEL retention, we transduced Arhgef1-

deficient OT1 cells with empty vectors (EV) or an activated TGFβ (aTGFβ) construct (Nakajima et al., 2000) prior to adoptive transfer to *Lm*-OVA infected recipients. The activated TGFβ has a mutation that limits association of the TGFβ small latent complex with the latent TGF binding protein-1 and tethering to the extracellular matrix (Nakajima *et al.*, 2000). Expression of this construct by T cells is expected to overcome the normally tight spatial restriction of active TGFβ (Deng et al., 2024). Activated TGFβ over-expression rescued CD103 expression (Fig. 4I) and prevented the decay of Arhgef1-deficient OTI CD8αβ IELs from the tissue at day 11 (Fig 4J). However, other key survival signals, such as IL15 or IL7, are needed to upregulate Bcl2 and prevent apoptosis (Jarjour *et al.*, 2025). We therefore tested the impact of Bcl2 over-expression and observed a rescue in IEL frequency but no increase in CD103 expression (Fig. 4K, and L and Suppl. Fig. S4E). Collectively these data suggest that Gα13 signaling is required for proper cell migration and positioning in the intestine for CD8αβ T cells to access niche-restricted cytokines, such as TGFβ, that support Bcl2 and CD103 upregulation and formation of long-lived Trm IELs.

Gα13-coupled GPCR CRISPR screen identifies role for GPR132 in IEL homeostasis.

Based on an assessment of RNAseq data from CD8αβ IEL for GPCR expression (Suppl. Fig. S5A), together with evidence curated from the literature regarding potential Gα13-coupling, we identified a set of 12 candidate GPCRs for in vivo testing. BM from Cas9-transgenic mice was transduced with retroviral constructs encoding pairs of sgRNA against individual GPCRs, Gna13 or control vectors (with Thy1.1 and BFP reporters), and used to reconstitute irradiated WT mice. Small intestinal IEL analysis of the 8 week reconstituted chimeras confirmed the efficacy of Gna13 targeting in reducing TCRαβ IEL (Fig. 5A). Of the 12 GPCRs, GPR132 targeting led to a significant reduction in IEL (Fig. 5A). Mixed BM chimeras generated using BM from GPR132$^{-/-}$ (Le et al., 2001) and WT mice showed reduced representation of GPR132-deficient CD8αβ T cells amongst IEL and LP cells, but not spleen cells (Fig. 5B, C and Suppl. Fig S5B). In transwell migration assays, WT CD8αβ IEL migrated to LPC and this response was lost in GPR132-deficient IEL (Fig. 5D). Gα13-deficient CD8αβ IEL failed to migrate to LPC (Fig. 5E). The LPC promigratory activity on CD8αβ IEL was also Arhgef1-dependent (Fig. 4F). Arhgef1 facilitates the exchange of GDP to GTP for the small GTPase RhoA which activates the ROCK1/2 kinases (Aittaleb *et al.*, 2010; Siehler, 2009). Treating CD8αβ IELs with the ROCK inhibitor, Y-27632, blocked migration in a dose dependent manner (Suppl Fig. S5C) and the ability of CD8αβ IELs to migrate to LPC (Fig. 5G). These findings provide evidence that GPR132 is a receptor acting upstream of Gα13, Arhgef1, and ROCK1/2 in CD8αβ IEL that contributes to their migration and competitive fitness. Nevertheless, GPR132 deficiency did not cause as severe a CD8αβ IEL loss as Gα13- or Arhgef1-deficiency. Three other Gα13 coupled receptors with known ligands, GPR55 and LPARs 5 and 6, were highly expressed by CD8αβ IELs (Suppl. Fig. S5A). Although CRISPR-targeting of these receptors did not lead to a loss of CD8αβ IELs alone, we observed their ligands, LPI and LPA, respectively, inhibited IEL migration in a Gα13 dependent manner (Suppl. Fig. S5D). It is therefore possible that combinations of these receptors signal through Gα13 to maintain the CD8αβ+ IEL populations.

IEL loss due to Gα13 deficiency is associated with more severe colitis and reduced rectal tumor control

We next investigated the impact of Gα13-deficiency on susceptibility to inflammatory intestinal conditions. We first subjected Gα13-deficienct mice to dextran sodium sulfate (DSS) induced colitis. Following 5 days of exposure to 2% DSS in the drinking water, Gα13ΔVav mice showed significantly greater weight loss (Fig. 5A), more intestinal pathology (Fig. 5B) and greater colon shortening compared to control mice (Fig. 5C). Similar weight loss findings were made with Gα13ΔCD4 mice (Fig. 5D) suggesting Gα13 signaling in T cells maintains the intestinal barrier and protects the host from chemical-induced damage. To test the impact of Gα13-pathway deficiency in an intestinal tumor setting, we used the colorectally implanted MC38 tumor cell model (Richon et al., 2023; Zhao et al., 2017; Zigmond et al., 2011). Gα13ΔCD4 mice suffered greater weight loss than littermate control mice following tumor implantation (Fig. 5E). To investigate tumor specific CD8 T cell responses, we rectally implanted MC38 cells expressing OVA in T cell-deficient mice and transferred an equal mixture of CD45.2 Arhgef1+/- OTI and CD45.1/.2 Arhgef1-/- OTI cells. Transferred control and Arhgef1-deficient OT1 T cells homed to the tumor site similarly at day 3 (Fig, 5F). At day 10, the control cells persisted whereas the Arhgef1-deficient cells disappeared (Fig. 5F). These findings provide evidence that Gα13 function in $CD8^+$ IEL contributes to promoting intestinal barrier integrity and anti-tumor immunity.

DISCUSSION

Our findings establish a critical role for Gα13 and its downstream effector Arhgef1 in the homeostasis of intestinal CD8 T cells, including developmentally programmed CD8αα γδT cells and αβT cells and antigen-induced CD8αβ Trm cells. G13-pathway null cells show deficiencies in key gene expression programs and they undergo increased apoptosis. Imaging analysis shows Gα13 is needed to support IEL migration and positioning. We propose that Gα13 signaling supports intestinal CD8αα and CD8αβ T cell migration behaviors that are necessary for receipt of differentiation or survival signals, including IL15 for γδT cells and TGFβ for CD8αβ T cells. We identify GPR132 as a Gα13-coupled receptor that promotes IEL migration and contributes to CD8αβ IEL homeostasis. The strong intestinal T cell defect in Gα13-pathway deficiency is associated with exacerbated DSS-induced colitis and defective anti-tumor immunity. Based on the magnitude and breadth of the intestinal CD8 T cell loss caused by G13-pathway deficiency, and its selectivity to the intestine, targeting this pathway may have therapeutic potential for treatment of T cell driven intestinal inflammatory diseases.

Studies in IL15 and IL15Rα deficient mice established that IL15 is critical for γδT IEL and contributes to maintaining CD8αα αβT IEL (Kennedy et al., 2000; Lodolce et al., 1998; Mortier et al., 2009; Schluns et al., 2004). Our finding that the γδT IEL remaining in Gα13-deficient mice have reduced IL15 pathway activity suggests Gα13 supports migration behaviors needed for accessing IL15. Spatial gene expression analysis revealed IL15 is more abundant near the tips of villi than the crypts (Reina-Campos *et al.*, 2025). The few γδT IEL remaining in Gα13ΔVav mice were near the crypts, perhaps indicating poor access to $IL15^+$ tips. Since IL15

promotes γδT IEL motility in vivo (Hu *et al.*, 2018), reduced access of Gα13-deficient γδT cells to IL15 may lead to a negative feedback loop and amplified cell loss. The inefficient movement of antigen-responding CD8αβ OT1 T cells to the tips suggests a shared requirement for Gα13 in this migration behavior. Recent work established that IL7 cooperates with IL15 to maintain intestinal CD8αβ Trm IEL (Jarjour *et al.*, 2025). IL7 is expressed by intestinal lymphatics and heterogeneously by intestinal epithelial cells, and spatial transcriptomics indicates greatest abundance mid-way along the crypt-villus axis (Hara et al., 2012; Reina-Campos *et al.*, 2025; Shalapour et al., 2010; Watanabe et al., 1998). It is possible that limited access to both IL7 and IL15 contributes to poor survival of all Gα13-deficient CD8 IEL types. Reduced IL7 and IL15 signaling may contribute to reduced Bcl2 expression (Jarjour *et al.*, 2025; Nakazato et al., 2007; Rathmell et al., 2001) and thus increased apoptosis of G13-pathway deficient cells.

TGFβR signaling in CD8αβ T cells has a well-established role in the maturation and maintenance of Trm IEL. In studies with LCMV infection and LCMV-specific P14 TCR transgenic T cells and OT1 T cells in the *Lm*-OVA model, Tgfbr2-/- cells arrive to the intestine in normal numbers one week after infection but then rapidly decay (Borges da Silva *et al.*, 2020; Sheridan *et al.*, 2014; Zhang and Bevan, 2013). We find the behavior of Arhgef1Δ OT1 cells in the oral *Lm*-Ova model has similar kinetics. In accord with a shared pathway, Arhgef1Δ OT1 cells in the intestine at day 8 have a reduced TGFβ gene expression signature and they can be rescued by TGFβ over-expression. The sources of TGFβ needed for intestinal CD8αβ T cells are not clear though many cell types express one or more of the TGFβR ligands (TGFβ1, TGFβ2 and TGFβ3) (Reina-Campos *et al.*, 2025). A critical requirement for TGFβ to signal is that it must be activated from a latent state. TGFβ activators include integrins αvβ6 and αvβ8 (Deng *et al.*, 2024). Notably, αvβ6 is more abundant at the tips of intestinal villi than in the crypts ((Ducceschi et al., 2014) and Suppl. Fig. S5E). In mice lacking Itgb6 (the gene encoding β6) and infected with LCMV, P14 cells reached the intestine in normal numbers at one week but were markedly reduced in the epithelium at day 42 (Mohammed et al., 2016). We suggest that Gα13 and Arhgef1 are needed for CD8αβ T cells to travel towards the tip of intestinal villi to receive adequate TGFβ exposure for their maturation and maintenance. In accord with exposure to active TGFβ being higher nearer the villus tip, spatial gene expression analysis showed higher amounts of TGFβ-induced transcripts in CD8 Trm cells nearer the tip (Reina-Campos *et al.*, 2025). However, we do not exclude other possibilities such as a role for Gα13 in supporting interactions in the crypt that favor TGFβR stimulation and trigger migration toward the tip and exposure to further TGFβ.

In our gene expression analysis of Gα13-deficient CD8αα αβT cells and Arhgef1-deficient CD8αβ Trm cells, the transcriptional regulators Nr4a2 and JunB were significantly less expressed. Using shRNA knockdown or conditional knockout, Nr4a2 and JunB were shown to be required for intestinal CD8 Trm and CD8αα IEL homeostasis (Kurd et al., 2020; Xing et al., 2024). Gα13-pathway mediated induction of Nr4a2 and JunB may therefore contribute to IEL homeostasis.

The nuclear hormone receptor AHR is important for γδT and CD8αα αβT IEL homeostasis and contributes to CD8αβ Trm formation (Dean et al., 2023; Li et al., 2011; McDonald *et al.*, 2018).

We did not observe expression of several classical AHR targets (Jackson et al., 2015) in IEL such as Cyp1a1, Cyp1b1, or Cyp1a2, while Ahrr and Tiparp expression was not affected. However, several genes identified as AHR targets in in vitro generated CD8 Trm-like cells (Dean *et al.*, 2023), including Itgae, S1pr5, Klrg1, and Eomes, were differentially expressed in Arhgef1-deficient OT1 d8 IEL, indicating a possible defect in AHR function in the absence of Gα13-pathway signaling. This might occur due to mispositioning and reduced access to AHR ligands or defects in AHR cooperating factors. One study reported Gα13 interacts with AHR-interacting protein (AIP) to promote AHR degradation (Nakata et al., 2009). However, our data do not provide evidence for increased AHR pathway activity in the absence of Gα13, making it unlikely that Gα13 acts in IEL by directly destabilizing AHR.

The endogenous ligands acting on GPR132 are not well defined. While LPC can promote GPR132$^+$ cell migration ((Kabarowski *et al.*, 2001; Radu *et al.*, 2004; Wang *et al.*, 2005; Yang *et al.*, 2005) and this report), it will be necessary to establish means to prevent LPC production to determine the role it plays in IEL homeostasis. Other ligands reported for GPR132 include lactate, N-palmitoylglycine, 9(S)-hydroxy-10,12-octadecadienoic acid, epoxyeicosatrienoic acid, oxylipins, and the microbiome derived molecule commendamide (Chen et al., 2017; Cohen et al., 2015; Lahvic et al., 2018; Obinata et al., 2005; Wang et al., 2023). It will be of interest to test if the contribution of GPR132 to IEL homeostasis depends on the microbiome. In accord with a role in IEL function, GPR132-deficiency exacerbated DSS-induced colitis (Frasch et al., 2016).

As well as promigratory actions in response to GPR132 ligands, Gα13 may guide cell migration in the villi by sensing cues that engage migration inhibitory responses. In addition to LPI (Sumida *et al.*, 2017), we found that LPA mediated IEL migration-inhibition in transwell assays. Although we did not detect an effect on IEL homeostasis of CRISPR-mediated Lpar5 or Lpar6 targeting, we do not exclude redundant actions of these receptors. Future studies in combined Gα13-coupled receptor deficient mice will be needed to address possible receptor redundancy.

How Gα13 supports the basal motility of IEL is an important question. We previously observed Gα13-dependent basal motility in germinal center B cells (Muppidi et al., 2015; Muppidi et al., 2014). It is possible that IEL (or other cells in the IEL preparation) are producing ligands for Gα13-coupled GPCRs that act in an autocrine or paracrine fashion to promote the basal motility. As well as its role downstream of Gα13-dominantly coupled GPCRs, Gα13 can be activated by Gαi-dominantly coupled GPCRs such as CXCR4 (Yagi et al., 2011). In this context, dual activation of Gαi and Gα13 is thought to reinforce ‘frontness’ and ‘backness’ (via Rac and Rho), respectively, and this in turn augments motility (De Belly et al., 2025; Xu et al., 2003). It is possible that Gα13 in IEL generates cell polarity even in the absence of external stimuli. Notably, isolated CD8$\alpha\alpha$ IEL have an amoeboid morphology compared to the round shape of isolated LN T cells (Takei et al., 2020) consistent with an intrinsically motile state.

While we favor a model where the action of Gα13 in guiding cell migration is key to its role in IEL, we do not exclude other possible mechanisms of action. These could include signaling for gene induction (Siehler, 2009; Yang et al., 2020), supporting integrin activity needed for adhesive events (Francis et al., 2006; Rubtsov et al., 2005), influencing TCR signaling (Kumar et al., 2011), or limiting pAKT and mTOR activity (Green and Cyster, 2012; Nguyen et al., 2024)

to enable the cells to be maintained in a partially activated (poised) state (Konjar et al., 2018; Kurd *et al.*, 2020). Some studies have noted interactions between Gα13 and Itk, a kinase that functions downstream of the TCR and has an important role in IEL homeostasis (Cho et al., 2020; Huang et al., 2013). However, Itk inhibition reduced α4β7 and CCR9 induction under gut tropic culture conditions (Cho *et al.*, 2020), a phenotype not observed for Gα13-deficiency, making it unlikely that Gα13 and Itk are acting in the same pathway in IEL.

γδT cell deficiency is associated with more severe DSS-induced colitis (Chen et al., 2002; Sun et al., 2017; Tsuchiya et al., 2003). Mice lacking αβT cells were also found to suffer more severe DSS-induced colitis (Tsuchiya *et al.*, 2003). The exacerbated colitis observed in Gα13ΔVav mice and Gα13ΔCD4 mice is in accord with these findings. γδT cells contribute to tissue repair by producing KGF1 (Chen *et al.*, 2002; Meehan et al., 2014). The mechanism by which αβT IEL contribute to restoring epithelial integrity and the role of Gα13 signaling in this process requires further investigation.

Intrarectal implantation of the MC38 colon tumor line (derived from a C57BL/6 grade III adenocarcinoma (Corbett et al., 1975)) provides a model for colorectal cancer and is associated with T, B and myeloid cell recruitment (Richon *et al.*, 2023; Zhao *et al.*, 2017; Zigmond *et al.*, 2011). Our findings indicate Gα13 pathway activity promotes tumor infiltrating CD8 T cell accumulation in colonic MC38 tumors. A recent CRISPR screen in human T cells identified Gα13 as a negative regulator of human T cell accumulation in skin tumors, an activity that may contribute to immune exclusion (Liu et al., 2025). We suggest that the dominant influence of Gα13 on tumor infiltrating T cell responses will differ by tissue site, with the essential role of Gα13 in intestinal IEL maturation and homeostasis playing a positive role in responses to intestinal tumors.

Using LCMV infection to broadly induce Trm cells, we found the Trm cell dependence on Gα13 was selective for the intestine, though we do not exclude roles in tissues we did not assess. The basis for this selectivity will require future exploration but it may in part reflect specialized migration requirements for intestinal Trm cells to access supportive niches. Beyond Trm cells, prior work on Gna13f/f CD4Cre mice identified a ~2-fold deficiency of Tfh cells in response to immunization, LCMV infection or allergen exposure (Kuen et al., 2021). Importantly, the impact of Gα13-deficiency on intestinal CD8 T cells was substantially more marked than the findings for Tfh cells. The selective dependence of intestinal CD8 T cells on Gα13 signaling makes this pathway of particular interest for therapeutic targeting in the context of T cell-driven inflammatory intestinal diseases.

Acknowledgements

We thank Dario Vignali (University of Pittsburgh, PA) for E8iCreERT2 mice. ZME was supported by T32 AI007334 and is supported by a Cancer Research Institute Irvington postdoctoral fellowship. JGC is an Investigator of the Howard Hughes Medical Institute. This work was supported in part by NIH grant R01 AI40573 and NHLBI R35HL161241.

MATERIALS AND METHODS

CONTACT FOR REAGENT AND RESOURCE SHARING

Further information and requests for resources and reagents should be directed to and will be fulfilled by the Lead Contact, Jason Cyster (Jason.cyster@ucsf.edu).

EXPERIMENTAL MODEL AND SUBJECT DETAILS

7-12 week old littermate mice were used for experiments, co-housed in specific pathogen-free conditions, at University of California San Francisco Laboratory of Animal Research Center. C57BL/6J, B6.SJL-*Ptprc*^{a} *Pepc*^{b}/BoyJ, B6.Cg-*Commd10*$^{Tg(Vav1\text{-}icre)A2Kio}$/J, Tg(Cd4-cre)1Cwi/BfluJ, B6.129S-*Tcrd*$^{tm1.1(cre/ERT2)Zhu}$/J, B6.129P2-*Tcrb*^{tm1Mom} *Tcrd*^{tm1Mom}/J, B6(C)-*Gt(ROSA)26Sor*$^{em1.1(CAG\text{-}cas9*,\text{-}EGFP)Rsky}$/J, B6.Cg-*Gt(ROSA)26Sor*$^{tm6(CAG\text{-}ZsGreen1)Hze}$/J (Ai6), B6.Cg-*Gt(ROSA)26Sor*$^{tm14(CAG\text{-}tdTomato)Hze}$/J (AI14), C57BL/6-Tg(TcraTcrb)1100Mjb/J were obtained from the Jackson Laboratory. Gna13fl/fl (Ruppel et al., 2005) and Arhgef1-/- mice (Francis *et al.*, 2006) on a C57BL6/J background were from an internal colony. GPR132 deficient mice (Le *et al.*, 2001), B6.129X1(C)-*Gpr132*^{tm1Witt}/J, were a gift from Li Yang at East Carolina University and were originally generated at UCLA in the laboratory of Owen Witte. E8icreERT2 mice (Andrews *et al.*, 2021) were a gift from Dario Vignali at University of Pittsburgh. For BM chimeras, mice were lethally irradiated by 450 rad x-ray irradiation in two-doses 3 hours apart and transferred retroorbital with at least 5X10^6 BM cells from donors of the indicated genotype. Mice were analyzed 8 weeks after reconstitution. All animal procedures were approved by the UCSF Institutional Animal Use and Care Committee.

Tamoxifen treatments

Ga13fl mice were crossed to TCRδCreERT2 (ΔTCRδ) and E8iCreERT2 (ΔCD8α) and Ai6 or Ai14 reporters for inducible Ga13 knockout studies. We used homozygous TCRdCreERT2 mice to improve the deletion efficiency and heterozygous E8icreERT2. We first verified that our tamoxifen regimen of Cre– mice did not change IEL numbers (unpublished observations). To control for any Cre leakiness, we compared Cre expressing mice not treated with tamoxifen (Control) to Cre expressing mice (ΔTCRδ or ΔCD8a) treated with tamoxifen. Tamoxifen (Sigma) was resuspended overnight at 20mg/ml in corn oil, shaking at 37°C in the dark, and 100ul was injected i.p. in the flank. Gα13ΔCD8α mice underwent 3 TAM treatments 24 hours apart for 6mg tamoxifen total, and Gα13ΔTCRδ mice underwent 5 TAM treatments for 10mg total tamoxifen/ mouse. For two photon imaging studies, we utilized Gna13fl/+ TCRδCreERT2 Ai14 (Control) mice compared to Gna13fl/fl TCRδCreERT2 Ai6 (Gα13ΔTCRδ) mice.

MC38 colorectal cancer model

For MC38 orthotopic colorectal cancer studies, we utilized a published method of mechanical intestinal epithelial injury and rectal injection of tumor cells to facilitate colon tumor engraftment (Richon *et al.*, 2023). MC38 expressing OVA was grown in complete DMEM to 80% confluency

at 37°C and 5% CO2, spun down and resuspended in PBS. Prior to the procedure mice were fasted for 6 hours to ensure minimal colon content. Recipient mice, Gα13fl, Gα13ΔCD4, or TCRbd-/-, were anesthetized with isoflurane and underwent rectal brushings with an interdental toothbrush dipped in EDTA that was prewarmed to 37°C to gently remove intestinal crypts. Crypts were examined under a light microscope to ensure similar brushings between mice. $2x10^6$ MC38-OVA cells were injected with a pipette tip intrarectally in 50ul of PBS and a plug was created with 20ul of Vetbond Tissue Adhesive (3M) to prevent the cells leaking from the rectum. Mice were kept under 1% isofluorane for 10min with a warming pad, moved back to cage, and 4 hours later the plug was gently removed. Mice were weighed daily and weight loss relative to initial weight was calculated. Due to some inevitable inherent variability in brushing strength and tumor engraftment with this procedure, mice that did not have visible tumor engraftments one week after the procedure were removed from analysis.

Intravital microscopy of the mouse small intestine

Mice were anesthetized with ketamine/xylazine (60/20 mg/kg, i.p.), and the abdominal area was shaved and prepared for surgery. Anesthesia was maintained with 1% isoflurane delivered in oxygen (1 L/min) through nosecone. Mice were positioned supine on a heating pad maintained at 37 °C. A small laparotomy was performed by incising the abdominal skin and underlying fascia to expose a short segment of small intestine. The mid-small intestine (jejunum or proximal ileum) was exteriorized and opened along the antimesenteric border using a cautery pen (Bovie high-temperature cautery pen, fine tip; ref. AA25) to expose the mucosal surface. The tissue was gently repositioned with a saline-moistened cotton-tipped applicator such that the mucosal surface faced upward. A 3D-printed imaging window (prepared as previously described (Cleary et al., 2025)) connected to a suction device was lowered onto the exposed tissue, and negative pressure (−20 mmHg) was applied to immobilize the intestinal segment against the coverslip during imaging.

Intravital imaging was performed on a Nikon A1R microscope equipped with a CFI75 Apochromat 25XC water-immersion objective and a high-resolution galvano scanner (UCSF Biological Imaging Development CoLab). Multiphoton excitation was provided by a Mai Tai DeepSee IR laser (950 nm). Emitted fluorescence was collected through 440/80-, 525/50-, and 600/50nm emission filters. Images were acquired at either 512 × 512 or 1,024 × 1,024 pixel resolution (when motion stability permitted). Time-lapse z-stacks spanning 9-12 μm were collected with 4-μm z-steps for 25-30 min. Raw image data were processed using the NIS.ai module in NIS-Elements (Nikon) to enhance signal-to-noise ratio.

Processed files were imported into Imaris 9.6.0 (Bitplane) for video rendering and cell tracking. IELs were identified and tracked using the built-in autoregressive spot-tracking algorithm. Tracks were filtered based on duration and total track length to exclude tracking artifacts. Automated tracking results were visually inspected and manually corrected when necessary. Mean track velocity was calculated directly from Imaris outputs and confinement ratio was defined as the ratio of track displacement to total track length (displacement/track length).

***Listeria monocytogenes* infections**

$2x10^9$ CFUs of *Listeria monocytogenes*, strain Lm^{InlA}-OVA, were orally inoculated into mice by gavage in 200ul of PBS after growing to an OD of 0.57. Infections occurred the day after adoptive T cell transfers or 2-3 hours after when cells were sorted. Mice were analyzed 8 days after infection for effector response or 28 days after for memory T cell response.

DSS colitis

2% DSS (MW ca 40000, Thermo Scientific) was administered ad libitum in the drinking water to Ga13ΔVav and Ga13ΔCD4 and littermate control mice. Mice were kept on DSS water for five days, followed by regular water for three days and euthanized. Weight was recorded every day at the same time throughout the duration of the DSS protocol and data were graphed as % of initial weight.

Isolation of intraepithelial lymphocytes (IEL), and lamina propria (LP) cells from the intestine

To isolate IELs for downstream flow cytometry or sequencing analysis, 14 cm of the small intestine from the stomach was excised and left over segments were discarded. The entire colon was taken after the cecum to the rectum. The Peyers patches were removed, the intestine was opened longitudinally, cut into 1cm pieces, and added to Hanks' Balanced Salt Solution media containing 10mM of HEPES buffer, 5mM of EDTA, and 1mM of DTT. The intestine pieces underwent two 20min shakes at 250RPM at 37C. The IEL cells were strained and then underwent a 40% percoll density gradient centrifugation step to remove dead cells and debris as previously described (Abadie et al., 2020). LP cells underwent two further 20min shakes at 250RPM at 37C with RPMI, 10% FBS, 20ug/ml DNase1, and 100U/mg of Collagenase VIII (Sigma C2139). Following the two shakes the LP underwent a percoll density gradient spin similar to the IELs. A fraction of the IELs and LP cells were taken for flow cytometry staining.

Flow cytometry

The cells were first stained with FC block (CD16/32) to block nonspecific binding, and then with Zombie NIR (Biolegend) for 15min at 4°C to exclude dead cells. Next the cells were stained for cell surface markers for 25min at 4°C. For AnnexV staining the cells were then stained with AnnexV-PE for 15min at 25°C in 1X binding Buffer (BD, 556454), washed and resuspended in the binding buffer and then the data were quickly acquired using Aurora Cytek. The antibodies used are indicated in Key resources table. The following antibodies and clones were purchased from Biolegend: CD45.2 BV421 (104), CD45.1 BV605 (A20), CD4 BV605 (GK1.5), CD44 PE-Cy7 (IM7), CD62L PE (MEL-14), Epcam PerCP-Cy5.5, AF488 (G8.8), CD3ε AF700 (145-2C11), CD8α APC-fire 750 (53-6.7), TCR Va2 APC (B20.1), CD103 PE-cy5 (2E7). The following antibodies and clones were purchased from BD: CD8β BV480, BV421 (H35-17.2), TCRβ BUV737 (H57-597), vβ5.1/5.2 TCR PE (MR9-4). The following antibodies and clones were purchased from Thermo Fisher: TCRγδ PE-cy7, AF647 (eBioGL3). Counting beads were added to determine absolute cell numbers in the original sample / amount of tissue taken. The cells were run on Aurora (Cytek) and data were analyzed using FlowJo software (Treestar). All cells were gated FSC SSC, singlets, and live. IELs were first gated: CD45+ CD3+. TCRγδ+ (TCRgd

IELs) or TCRβ+ then CD4+ CD8α- (CD4 IELs). CD8α+ CD4- then CD8β+ (CD8αβ IELs) or CD8β– (CD8αα IELs).

Retroviral constructs and transductions

Bcl2 retroviral construct was made by inserting the murine open reading frame into the MSCV2.2 retroviral vector followed by an IRES and a GFP expression marker. The active TGFβ construct was generated by making a cysteine to serine substitution in human TGFβ1 at amino acid residue 33 (Nakajima *et al.*, 2000) and cloned this into MSCV2.2 retroviral vector followed by an IRES and Thy1.1 reporter. For the G protein-coupled-receptor screen, single-guide RNA (sgRNA) sequences were cloned into the pTR-MSCV-IRES-Thy1.1 or pTR-MSCV-IRES-BFP vector. SgRNA sequences were selected using Benchling's CRISPR Guide tool and 2 guides were designed for each GPCR. To produce retroviruses, Platinum-E packing cells (Cell Biolabs) were grown to 75% confluency in a 10cm tissue culture dish and transfected with 10ug plasmid/25ul of Lipofectamine 2000 (Thermo Fisher) in OptiMEM following manufacturer's protocol. ViralBoost (Alstem) was added to the media 16 hours later and retrovirus containing supernatants were collected 48 and 72 hours after transfection, filtered through a 0.45um filter to remove debris, and concentrated 10 fold with Retro-X concentrator (Takara). For BM transductions, constitutive CAS9-GFP expressing donor mice were injected i.p. with 3 mg of 5-fluorouracil (Sigma), BM was collected after 4 days and cultured with complete DMEM supplemented with 20 ng/ml of interleukin-3 (IL-3), 50 ng/ml of IL-6, and 100 ng/ml of stem cell factor. BM cells were spin-infected (1000*g*, 2 hours, 32°C) at day 1 and day 2 and injected into irradiated recipients after the second transduction. For T cell transduction, CD8αβ T cells were activated with aCD3/CD28 T cell activator Dynabeads (Gibco) and 60U human IL-2 (NCI) in complete RPMI for 24 hours. The T cells underwent 2 spinfections (1000*g*, 2 hours, 32°C) with retrovirus 24 and 48 hours later on 20ug/ml Retronectin (Takara) coated 6 well plates.

Adoptive transfers

OTI T cells were enriched from the spleen, MLN, and iLN of Arhgef1+/- or Arhgef1-/- OTI donor mice from using negative selection anti-biotin beads (STEMcell Technologies) after staining with the following biotinylated antibodies: aCD4, aCD11b, aCD11c, aCD49b, aF4/80, aTCRγδ, aTER119, aGR1, aI-A/I-E, aB220. Cells were counted on a hemocytometer, and 50,000 OTI T cells were transferred to CD45.1 mice retro-orbitally. For Bcl2 mixed overexpression, 50,000 GFP+ EV-GFP or BCL2-GFP transduced OTI cells were sorted and mixed with 50,000 GFP– cells and transferred to CD45.1 mice retro-orbitally. 1x10^6 mixed congenically marked (CD45.1/.2 or CD45.2/.2) Arhgef1+/- or Arhgef1-/- OTIs were transferred to TCRbd-/- mice three days after MC38 engraftment retro-orbitally for tumor studies.

Transwell migration assay

IELs were counted and resuspended in migration medium (0.5% fatty-acid free BSA, 10mM Hepes RPMI) at 4×10^6cells / ml. Transwell filters (6 mm insert, 5 μm pore size, Corning) were placed on top of each well, and 100 μl containing 4×10^5 cells were added to the transwell insert. No ligand (Nil), lysophosphatidylcholine (LPC) 30uM, lysophosphatidic acid (LPA) 10uM, or CCL25 (1ug/ml) were added to the media at the bottom of the transwell. The cells were

allowed to migrate for 3 hrs at 37°C with 5% CO2 and the cells in the bottom well were stained and counted by flow cytometry.

Histology

8 cm of jejunum or whole colon were excised and opened longitudinally. Intestinal content was removed. Starting from the most distal end and with the luminal side facing upwards, tissues were rolled into Swiss rolls and pinned together. For H&E staining, tissues were fixed with 10% formalin (Sigma-Aldrich), transferred to 70% ethanol 24 hours later, embedded in paraffin, and cut at 5 µm thickness at Histowiz laboratory, NY. For immunofluorescence staining, tissues were fixed with 1.5% PFA in PBS (Electron Microscopy Sciences) for 4-6 hours, washed in PBS, and transferred to 30% sucrose overnight at 4°C to dehydrate the tissue. The tissues were embedded in OCT and 1µum sections were cut with a cryostat. To stain the slides, the tissue sections were first washed for 10min in PBS, then permeabilized and blocked with 0.1% Triton X-100 (Sigma-Aldrich) 0.1% BSA and 5% normal rat and hamster sera (Jackson Immuno Research) in PBS for 1 hour at room temperature. Antibodies were added to the blocking solution at 1:200 for TCRγδ-AF647, 1:200 CD8β-BV421, 1:500 EpCAM-AF488, and CD45.2 AF594 and stained overnight at 4°C. The slides were then washed three times with permeabilization buffer for 30 min total, briefly rinsed in water, and mounted with Aqua-mount (Thermo Fisher). The slides were imaged with Leica STELLARIS confocal microscope.

IF Imaging Analysis

Tiled images of 7 µm-thick jejunal sections were acquired using a Zeiss Axio Observer Z1 inverted microscope equipped with a Zeiss AxioCam 506 mono camera and a Zeiss Plan-Apochromat 10×/0.45 objective lens. Image acquisition and stitching were performed using ZEISS ZEN 2 software. Stitched images were imported into QuPath v0.6.0. for downstream analysis. Automated cell detection was performed using the QuPath cell detection module with fixed parameters across all samples. Detection settings were optimized to exclude artifacts based on cell size and signal intensity thresholds. To quantify CD45.2+ OT1 T cell distribution along the crypt-villus axis, line annotations (arrows) were manually drawn from the top of the crypt to the tip of the villus. Only villi meeting predefined inclusion criteria were analyzed. Specifically, villi were required to: (i) exceed 70 µm in length; (ii) exhibit preserved morphology without horizontal or vertical collapse; (iii) be fully intact (not truncated); (iv) demonstrate EpCAM signal intensity allowing accurate crypt detection; (v) lack significant bending; (vi) not be in close proximity to adjacent villi that could confound assignment; and (vii) contain positively detected cells by QuPath. Using a custom script, each detected cell was assigned a relative position along its nearest villus axis via vector projection.
Cells located more than 50 µm from the annotated axis were omitted from analysis. The projected position of each cell was normalized along the length of the villus axis (0-1) and categorized into three bins representing spatial compartments: Low (0-.333), Medium (.333-.666), and High (.666.-1) villus regions.

Cell sorting for RNAseq

For cell sorting, 4000+ TCRβδ+ TCRαβ–, 4000 TCRαβ+ CD8α+ CD4- and 4000 CD4+ IELs, were sorted with Aria Fusion (BD Biosciences) from 3 pooled Gα13fl or Gα13ΔVav mice that

were hash-tagged during the surface staining to distinguish genotypes using CD45/MHCI (Biolegend TotalSeq). Samples were loaded on 10x Chromium Controller (10X Genomics) immediately after sorting. For bulk sequencing of CD8αβ IELs 100 TCRαβ CD8αβ+ IELs were sorted into SmartSeq 1X Reaction mix with 3' SMART-Seq CDS Primer II (TAKARA). Libraries were generated with SMART-seq v4 (TAKARA) at UCSF Genomics facility and sequenced on NovaSeq (Illumina).

RNAseq

For scRNAseq, samples were run on a 10X Chromium chip with 3′ v.2 chemistry (10X Genomics) as per the manufacturer's instructions by the UCSF Institute for Human Genetics Sequencing Core. Transcripts captured in all the cells encapsulated with a bead were uniquely barcoded using a combination of a 16 bp 10x Barcode and a 10 bp unique molecular identifier (UMI). cDNA libraries were generated using the Chromium™ Single Cell 3' Library & Gel Bead Kit v3 (10x Genomics) following the detailed protocol provided by the manufacturer. Libraries were sequenced with the NovaSeq 6000 platform (S1 Cartridge, Illumina) in 150 bp paired-end mode. The hashtag library was demultiplexed using CellRanger software (version 7.0.0) (Zheng et al., 2017). Aligned reads were used to quantify the expression level of mouse genes and generation of gene-barcode matrix. Subsequent data analysis was performed using Seurat R package (4.0.4) (Hao et al., 2021). Quality control was performed, and viable cells were selected by excluding cells with features lower than 1500 and above 4000, as well as cells having more than 3.5% of mitochondrial transcripts and more then 15000 transcripts. Control and Gα13ΔVav-derived cells were demultiplexed with the HTODemux function integrated in Seurat with standard settings. All doublets were removed for the analysis. 2000 most variable genes used for the anchoring process were used for downstream analysis to calculate principal components, after log-normalization and scaling. Principle component analysis (PCA) was used for dimensionality reduction and to visualize a uniform manifold approximation and projection (UMAP) of the identified clusters. P-values comparing gene expression of clusters and samples were calculated with the FindMarker function in Seurat. Gene list was generated using an adjusted p-value cutoff <0.05 and expression in the indicated cluster cutoff >25. For GSEA of TGFβ and IL15 induced genes, log2 fold change (LFC) and adjusted p values (padj) were given as input to the fgsea() function from the fgsea R package (v.1.32.0), which implements a pre-ranked gene set enrichment analysis. The rankings of the genes were based on generated score calculated by LFC * -log10(padj).

Raw bulk RNA-seq data were processed using STAR (Dobin et al., 2013) and RSEM (Li and Dewey, 2011) in default settings. In short, raw fastq files were mapped to mm10 genome, and TPM was calculated using RSEM. Then the data was loaded into and further analyzed by DESeq2 (Love et al., 2014). Differential expressed genes were called with padj < 0.05 and abs(log2Foldchange) >= 0.6 (approximately fold change of 1.5). Enrichr (Chen et al., 2013) was used to perform pathway analysis of up-regulated genes and down-regulated genes, respectively, and selected significant biological pathways padj < 0.05 were plotted from MsigDB hallmark, WikiPathways, Gene Ontology, and KEGG databases.

Xenium spatial transcriptomics data were obtained from the publicly available dataset generated by (Reina-Campos *et al.*, 2025). Imaging files and transcript coordinate data from small intestinal tissue at day 8 post-LCMV infection were processed and plotted using the public analysis pipeline developed by the Goldrath Lab (available on GitHub).

FIGURE LEGENDS

Figure 1: Gα13 is required for intestinal IEL T cell homeostasis

A. t-SNE analysis of 35 color flow cytometry panel of the small intestine from Ga13fl (left) and Ga13ΔVav (right) mice.

B. Representative flow cytometry plot of the frequency of small intestinal intraepithelial TCRαβ+ and TCRγδ+ cells among CD3+ cells (left) and TCRαβ+ CD8αβ+ or TCRαβ+ CD8αα+ among CD8α+ CD4- cells (right) from Ga13fl and Ga13ΔVav mice.

C, D. Total small intestine (C) or colon (D) cell numbers of IEL subsets in Ga13fl and Ga13ΔVav mice.

E. Representative IF image from the small intestine of Ga13fl and Ga13ΔVav mice stained for TCRγδ (red), CD8β (white), and EpCAM (blue).

F. Representative flow cytometry plot of the Annexin V+ cell frequency among TCRγδ+ cells from Ga13fl and Ga13ΔVav mice

G. Mixed BM chimera analysis for indicated IEL types showing ratios of CD45.2+ Ga13fl (blue) or Ga13ΔVav (red) and CD45.1/2+ WT cells in WT recipients.

H. Same as in G except with CD45.2+ Arhgef1+/- (grey) and Arhgef1-/- (pink) with CD45.1/2+ WT.

I. Total numbers of small intestinal IEL subsets in Ga13fl and Ga13ΔCD4 mice.

All data are pooled from two independent experiments of N= 6-10 mice / group and represented as mean ± SEM. ****P<0.0001 , *** P<0.001, ** P<0.01, * P<0.05, t-test.

Figure 2: Conditional Gα13 deletion from IEL leads to cell loss and defective motility

A. Number of TCRγδ cells in the small intestine of WT mice (blue, Ga13ΔTCRδ – TAM) or inducible Ga13ΔTCRδ mice (yellow, Ga13ΔTCRδ + TAM) 3, 5, 7, 10 or 14 days after TAM treatment.
B. Number of TCRαβ+ CD8αα+ cells (left) or TCRαβ+ CD8αβ+ (right) in the small intestine from WT mice (blue, Ga13ΔCD8α – TAM) or inducible Ga13ΔCD8a mice (maroon, Ga13ΔCD8a + TAM) 1, 3, 5, 7 or 14 days after TAM treatment. In A and B, data are from three independent experiments.
C,D. Frequency of TCRγδ+ (C) or TCRαβ+ CD8αβ+ (D) IELs that migrated through a transwell without added ligands 7 or 5 days, respectively, after TAM treatment. Groups and coloring as in (A,B).
E. Experimental scheme of two-photon intravital imaging of the small intestine of Ga13ΔTCRδ ZsGreen mice 3, 7, 10, and 14 days after TAM treatment.
F. Track speed (μm/min) of ZsGreen+ TCRγδ cells in mice treated as in E.
G. Time series at day 3 and day 14 showing representative tracks at 0 and 15 minutes of imaging. White arrows highlight cells with marked tracks (white lines). See also Movies S1-S4.
H. Confinement ratio of TCRγδ cells (displacement/distance) determined from the tracks of cells at D3 or D14 after TAM.
I. Experimental scheme of mixed BM chimera two-photon intravital imaging of TCRγδ cells 14 days after TAM treatment. TCRβδ-/- recipient mice were irradiated and reconstituted with control BM (pink, Ga13fl/+ TCRdCreERT2+ tdTomato) mixed 1:1 with Ga13ΔTCRδ BM (green, Ga13fl/fl TCRdCreERT2+ ZsGreen).
J. Representative tracks over time (0, 2, 4, 6 min) of control (pink) and Ga13ΔTCRδ (green) TCRγδ cells from mice prepared as in I. White arrows highlight cells with marked tracks (white lines). See Movies S5 and S6.
K . Track speed (μm/min, left) and confinement ratio (right) of tdTomato+ control and ZsGreen+ TCRγδ cells in BM chimeric mice prepared as in (I).

Data are represented as mean ± SEM. ****$P<0.0001$, *** $P<0.001$, ** $P<0.01$, * $P<0.05$, t-test.

Figure 3: Gene expression profile of Gα13-deficient intestinal T cells

A. uMAP plot of 10X scRNA-seq data of matched numbers of IELs sorted from Ga13fl (left) and Ga13ΔVav (right) mice.

B. Dot plot of select DE genes from CD8αβ and TCRγδ T cell clusters of Ga13fl and Ga13ΔVav mice.

C. GSEA of IL15-induced signature (James *et al.*, 2021) in TCRγδ cells from Ga13ΔVav mice compared to Ga13fl mice.

D. Heatmap of select DE genes from SMARTseq of CD8αβ IELs from Ga13fl and Ga13ΔCD4 mice.

E. Pathway analysis for (left) upregulated and (right) downregulated genes, showing select differently expressed biological pathways from MsigDB hallmark, Gene Ontology, WikiPathways, and KEGG in CD8αβ IELs from Ga13fl and Ga13ΔCD4 mice. Padj<0.05.

F. Expression of Bcl2 (TPM, transcripts/million) in CD8αβ IELs from Ga13fl and Ga13ΔCD4 mice.

G. Retroviral BM chimeras with overexpression of EV-GFP (open circles) or Bcl2-GFP (filled circles) in Ga13fl (blue) and Ga13ΔVav (red) cells. Data are expressed as a ratio of GFP+/ GFP- of each group of TCRγδ (left) or CD8αβ (right) IELs. N = 3-5 mice/group and are representative of two independent experiments. Data are shown as mean ± SEM. ** *P*<0.01, * *P*<0.05, ANOVA with Tukey multiple comparisons.

Figure 4. G13 signaling controls the maturation and homeostasis of intestinal CD8αβ Trm

A. Upper: experimental scheme for analyzing effector vs memory intestinal Arhgef1+/- or Arhgef1-/- OTI T cell response following adoptive transfer and oral *Lm*-OVA infection. Lower: representative FACS plots of Arhgef1+/- and Arhgef1-/- OTI (Vα2+ CD45.2+) T cells among CD8αβ IEL 8 or 28 days after infection.

B. Absolute cell numbers of Arhgef1+/- and Arhgef1-/- OTI T cells 8, 11, 14, and 28 days after infection.

C. Frequency of Annexin V+ Arhgef1+/- or Arhgef1-/- OTI (Vα2+ CD45.2+) T cells by FACS 8 days after infection.

D. Number of GP33+ CD8αβ+ T cells 28 days after LCMV Armstrong infection of WT (or Ga13ΔCD4 mice (maroon) in small intestine (IEL), skin, liver, lung, and spleen.

E. Representative FACS plot of CD69+ and CD103+ GP33+ CD8αβ Trm cells in the IEL from WT or Ga13ΔCD4 mice.

F. GSEA of TGFβ induced signature (Reina-Campos et al. 2025) in CD8αβ T cells comparing Arhgef1+/- and Arhgef1-/- OTI T cells at day 8 of the *Lm*-OVA infection time course .

G. Frequency of CD103+ Arhgef1+/- and Arhgef1-/- OTI T cells 8 or 11 days after infection.

H. Left panels show representative IF images of small intestinal sections from recipients of Arhgef1+/- or Arhgef1-/- OTI T cells (CD45.2, green) at day 8 after infection, EpCAM (blue). Right graph shows summary frequency of OTI T cells found in the low, med, and high position of the villi.

I. Retroviral overexpression of aTGFβ-Thy1.1 and control EV-Thy1.1 in Arhgef1-/- OTI T cells. Left panels are representative flow plots showing frequency of CD103+ in Thy1.1+ OTI T cells for EV and aTGFβ groups at day 11 post infection. Right graph shows summary CD103 data.

J. Fold increase in the absolute number of reporter+ cells from (I).

K. Retroviral overexpression of Bcl2-GFP or control EV-GFP in Arhgef1-/- OTI T cells. The cells were mixed 1:1 with non-transduced Arhgef1-/- OTI T cells, transferred and analyzed at day 11 post infection.

L. Frequency CD103+ among GFP+ EV and Bcl2 OT1 cells from (K).

All data are pooled from two independent experiments of N= 4-6 mice / group and represented as mean ± SEM. ****$P<0.0001$, *** $P<0.001$, ** $P<0.01$, * $P<0.05$, t-test. H, ****$P<0.0001$, Fisher's exact test

Figure 5. Gα13-coupled GPCR CRISPR screen identifies role for GPR132 in IEL homeostasis

A. Retroviral CRISPR/CAS9 BM screen of selected GPCRs. Data are expressed as a ratio of sgRNA1- BFP+ and sgRNA2-Thy1.1+ among TCRαβ+ cells in the IEL/spleen. Control represents non-targeting guides.

B, C. Ratio of CD8αβ T cells in the IEL (B) or spleen (C) from mixed BM chimeras made with GPR132+/- or GPR132-/- (CD45.2) BM mixed 1:1 with WT (CD45.1/.2) BM.

D. Frequency of GPR132+/- or GPR132-/- CD8αβ IELs that migrate in response to no ligand (Nil) or LPC added at 30, 10, or 3 μM to the bottom of a transwell.

E. Frequency of CD8αβ IEL transwell migration to Nil, or LPC, of WT or inducible Ga13ΔCD8α cells 5 days after TAM treatment.

F. Frequency of CD8αβ IEL transwell migration to Nil or LPC of Arhgef1+/- or Arhgef1-/- OTI IEL at day 8 post *Lm*-OVA infection.

G. Transwell CD8αβ IEL migration to LPC (maroon) or no ligand (grey blue) in the absence (Nil) or presence of ROCK inhibitor added at indicated concentrations.

All data are pooled from two independent experiments of N= 4-10 mice / group and represented as mean ± SEM. ****P<0.0001 , *** P<0.001, ** P<0.01, * P<0.05, t-test.

Figure 6. IEL loss due to T cell Gα13 deficiency is associated with more severe colitis and reduced rectal tumor control

A. Weight loss over time of Ga13fl and Ga13ΔVav mice challenged with 2% DSS in the drinking water for 5 days.

B. Representative H&E from Swiss rolls of the colon of Ga13fl and Ga13ΔVav mice 8 days after DSS.

C. Colon length (cm) 8 days after DSS colitis in the indicated mice.

D. Weight loss over time of Ga13fl and Ga13ΔCD4 mice challenged with 2% DSS in the drinking water for 5 days.

E. Weight loss over time of Ga13fl and Ga13ΔCD4 mice challenged with intrarectal MC38 tumors.

F. Experiment scheme (top) of a mixed 1:1 Arhgef1+/- (CD45.2) and Arhgef1-/- (CD45.1/.2) OTI T cell transfer to TCRβδ-/- mice that were intrarectally implanted with MC38-OVA tumors. Representative FACS plot (bottom) of OTI T cells (vα2+ vβ5+) from the tumor 3 or 10 days after transfer, with Arhgef1 genotype identification based on CD45.1/2 staining.

All data are pooled from two independent experiments of N= 5-10 mice / group and represented as mean ± SEM. ****P<0.0001 , *** P<0.001, ** P<0.01, * P<0.05, t-test.

SUPPLEMENTARY FIGURE LEGENDS

Figure S1. Gα13 is required for intestinal IEL T cell homeostasis (related to Figure 1)

A. Small intestine LP cell numbers of T cell subsets in Ga13fl and Ga13ΔVav mice.

B. Representative IF image from the small intestine of Ga13fl and Ga13ΔVav mice stained for TCRγδ (red) and EpCAM (green).

C, D. Numbers of TCRγδ+ (C) or CD8αβ (D) T cells in the skin, liver, lung, spleen, and MLN of Ga13fl and Ga13ΔVav mice.

E. Number of CD8αα IEL precursors in the thymus of Ga13fl and Ga13ΔVav mice gated: CD4- CD8α– TCRβ+ CD5+ CD122+ H2kb+ PD1+ CD44lo.

F. Frequency of Annexin V+ cells among TCRγδ+ IEL.

G. Total numbers of small intestinal IEL subsets in Arhgef1+/- and Arhgef1-/- mice.

H. Representative FACS plot of IFNγ+ CD8αβ IELs in Ga13fl and Ga13ΔVav mice.

Figure S2. Conditional Gα13 deletion from IEL leads to cell loss (related to Figure 2)

A. Experimental scheme of tamoxifen (TAM) treatment in Ga13ΔTCRδ mice (left) and representative FACS plots of ZsGreen induction in TCRγδ IELs of homozygous and heterozygous CreERT2+ mice 7 days after start of TAM treatments.

B. Experimental scheme of tamoxifen treatment in Ga13ΔCD8α mice (left) and representative FACS plots of tdTomato induction in CD8αβ IELs of heterozygous CreERT2+ mice 3 days after start of TAM treatments.

C. Number of TCRγδ IELs in Ga13ΔCD8α mice, 1, 3, 5, and 7 days after start of TAM.

Figure S3. Single cell RNA-seq analysis of Gα13-deficient intestinal T cells (related to Figure 3)

A. uMAP of Seurat clusters from 10x RNAseq analysis of sorted IELs from Ga13fl and Ga13ΔVav mice.

B. uMAP of gene expression plots of Tcrd, Cd8a, Cd8b1, Cd4 and Mki67 from (A).

Figure S4. Intact induction of gut tropism but poor intestinal survival of Gα13-deficient CD8αβ T cells (related to Figure 4)

A. FACS plot of CCR9 and α4β7 levels in Ga13ΔVav CD8αβ T cells 5 days after activation in the absence (Nil) or presence of retinoic acid (RA) and TGFβ.

B. Frequency of CD8αβ IEL transwell migration to Nil or CCL25 of Ga13fl or Ga13ΔVav T cells 5 days after activation in gut tropic conditions.

C. Experimental scheme (top) of adoptive transfer of skewed gut tropic CD8αβ T cells generated as in (A) to CD45.1 WT recipients and analyzed 2, 5, and 10 days after transfer. Frequency of Ga13fl or Ga13ΔVav CD45.2 CD8αβ IELs recovered after transfer (bottom).

D. Example images used for quantitating transferred control or Arhgef1-/- OTI T cell distribution in small intestine of *Lm*-OVA infected recipients at day 8. Arrows indicate villi used for quantitation of CD45.2+ OT1 cells (green). Epithelium was detected with EpCAM (blue).

E. Representative FACS plot of IEL from mice that received Arhgef1-/- OTI cells transduced with control EV-GFP or Bcl2-GFP mixed equally with non-transduced cells, at day 11 post transfer to *Lm*-OVA infected hosts.

Figure S5. GPCR expression in CD8αβ IEL, impact of GPR132-deficiency and migratory response to lysophospholipids (related to Figure 5)

A. Top 50 GPCRs by FPKM expression from RNAseq of transferred WT OTI IELs 8 days post *Lm*-OVA infection.

B. Ratio of CD8αβ T cells in the LP from BM chimeras made with GPR132+/- or GPR132-/- (CD45.2) BM mixed 1:1 with WT (CD45.1/.2) BM.

C. Transwell migration assay of CD8αβ IEL incubated with no inhibitor (Nil) or Y-27632 (ROCK inhibitor) at the indicated concentrations. Migration was performed in the absence of chemoattractant.

D. Frequency of CD8αβ IEL transwell migration to Nil, LPA, or LPI, of control or inducible Ga13ΔCD8α cells 5 days after TAM treatment.

E. Distribution of transcripts for TGFβ-activating integrin chains Itgav, Itgb6 and Itgb8 in spatial RNAseq analysis of mouse small intestine at day 8 of LCMV infection, determined using data from (Reina-Campos *et al.*, 2025). Very few Itgb8 transcripts were detected.

Supplemental Movie Legends

Movies S1-S4. Real-time imaging of γδT IEL migration in small intestine of a Gna13f/f Ai6 TCRδCreERT2 mouse at various days after tamoxifen treatment. Each movie in the concatenated series is a 20-30-min time-lapse sequence (duration indicated on bottom right of movie) of 9-12µm *z*-projection images. ZsGreen+ IEL are in green and nuclei in blue (Hoechst). The epithelium surrounding the villi in the projection image can be identified by the uniform lines of labeled nuclei. The nuclei within the interior of the villi help identify the lamina propria. Time after tamoxifen treatment: Movie S1, day3; Movie S2, day 7; Movie S3, day 10; Movie S4, day 14.

Movies S5 and S6. Real-time imaging of γδT IEL migration in small intestine of a Gna13f/f Ai6 TCRδCreERT2 / WT Ai14 TCRdCreERT2 mixed BM chimeras at day 21 after tamoxifen treatment. Each of the concatenated movies is a 15-min time-lapse sequence of 9-12µm *z*-projection images. ZsGreen+ Ga13Δ γδT IEL are in green, TdTomato+ WT γδT IEL are in pink and nuclei in blue (Hoechst). The white lines show cell tracks. In some cases, the cell movement was too little to generate a visible track.

REFERENCES

Abadie, V., Kim, S.M., Lejeune, T., Palanski, B.A., Ernest, J.D., Tastet, O., Voisine, J., Discepolo, V., Marietta, E.V., Hawash, M.B.F., et al. (2020). IL-15, gluten and HLA-DQ8 drive tissue destruction in coeliac disease. Nature *578*, 600-604. 10.1038/s41586-020-2003-8.

Aittaleb, M., Boguth, C.A., and Tesmer, J.J. (2010). Structure and function of heterotrimeric G protein-regulated Rho guanine nucleotide exchange factors. Mol. Pharmacol. *77*, 111-125. 10.1124/mol.109.061234.

Andrews, L.P., Vignali, K.M., Szymczak-Workman, A.L., Burton, A.R., Brunazzi, E.A., Ngiow, S.F., Harusato, A., Sharpe, A.H., Wherry, E.J., Taniuchi, I., et al. (2021). A Cre-driven allele-conditioning line to interrogate CD4(+) conventional T cells. Immunity *54*, 2209-2217 e2206. 10.1016/j.immuni.2021.08.029.

Borges da Silva, H., Peng, C., Wang, H., Wanhainen, K.M., Ma, C., Lopez, S., Khoruts, A., Zhang, N., and Jameson, S.C. (2020). Sensing of ATP via the Purinergic Receptor P2RX7 Promotes CD8(+) Trm Cell Generation by Enhancing Their Sensitivity to the Cytokine TGF-beta. Immunity *53*, 158-171 e156. 10.1016/j.immuni.2020.06.010.

Chen, E.Y., Tan, C.M., Kou, Y., Duan, Q., Wang, Z., Meirelles, G.V., Clark, N.R., and Ma'ayan, A. (2013). Enrichr: interactive and collaborative HTML5 gene list enrichment analysis tool. BMC bioinformatics *14*, 128. 10.1186/1471-2105-14-128.

Chen, P., Zuo, H., Xiong, H., Kolar, M.J., Chu, Q., Saghatelian, A., Siegwart, D.J., and Wan, Y. (2017). Gpr132 sensing of lactate mediates tumor-macrophage interplay to promote breast cancer metastasis. Proc. Natl. Acad. Sci. U. S. A. *114*, 580-585. 10.1073/pnas.1614035114.

Chen, Y., Chou, K., Fuchs, E., Havran, W.L., and Boismenu, R. (2002). Protection of the intestinal mucosa by intraepithelial gamma delta T cells. Proc. Natl. Acad. Sci. U. S. A. *99*, 14338-14343. 10.1073/pnas.212290499.

Cho, H.S., Ha, S., Shin, H.M., Reboldi, A., Hall, J.A., Huh, J.R., Usherwood, E.J., and Berg, L.J. (2020). CD8(+) T Cells Require ITK-Mediated TCR Signaling for Migration to the Intestine. Immunohorizons *4*, 57-71. 10.4049/immunohorizons.1900093.

Cleary, S.J., Qiu, L., Seo, Y., Baluk, P., Liu, D., Serwas, N.K., Taylor, C.A., Zhang, D., Cyster, J.G., McDonald, D.M., et al. (2025). Intravital imaging of pulmonary lymphatics in inflammation and metastatic cancer. J. Exp. Med. *222*. 10.1084/jem.20241359.

Cohen, L.J., Kang, H.S., Chu, J., Huang, Y.H., Gordon, E.A., Reddy, B.V., Ternei, M.A., Craig, J.W., and Brady, S.F. (2015). Functional metagenomic discovery of bacterial effectors in the human microbiome and isolation of commendamide, a GPCR G2A/132 agonist. Proc. Natl. Acad. Sci. U. S. A. *112*, E4825-4834. 10.1073/pnas.1508737112.

Corbett, T.H., Griswold, D.P., Jr., Roberts, B.J., Peckham, J.C., and Schabel, F.M., Jr. (1975). Tumor induction relationships in development of transplantable cancers of the colon in mice for chemotherapy assays, with a note on carcinogen structure. Cancer Res. *35*, 2434-2439.

Dai, B., Hackney, J.A., Ichikawa, R., Nguyen, A., Elstrott, J., Orozco, L.D., Sun, K.H., Modrusan, Z., Gogineni, A., Scherl, A., et al. (2021). Dual targeting of lymphocyte homing and retention through alpha4beta7 and alphaEbeta7 inhibition in inflammatory bowel disease. Cell Rep Med *2*, 100381. 10.1016/j.xcrm.2021.100381.

De Belly, H., Gallen, A.F., Strickland, E., Estrada, D.C., Zager, P.J., Nagy, T.L., Burkhardt, J.K., Turlier, H., and Weiner, O.D. (2025). Long range mutual activation establishes Rho and Rac polarity during cell migration. bioRxiv. 10.1101/2024.10.01.616161.

Dean, J.W., Helm, E.Y., Fu, Z., Xiong, L., Sun, N., Oliff, K.N., Muehlbauer, M., Avram, D., and Zhou, L. (2023). The aryl hydrocarbon receptor cell intrinsically promotes resident memory CD8(+) T cell differentiation and function. Cell Rep *42*, 111963. 10.1016/j.celrep.2022.111963.

Deng, Z., Fan, T., Xiao, C., Tian, H., Zheng, Y., Li, C., and He, J. (2024). TGF-beta signaling in health, disease, and therapeutics. Signal Transduct Target Ther *9*, 61. 10.1038/s41392-024-01764-w.
Dobin, A., Davis, C.A., Schlesinger, F., Drenkow, J., Zaleski, C., Jha, S., Batut, P., Chaisson, M., and Gingeras, T.R. (2013). STAR: ultrafast universal RNA-seq aligner. Bioinformatics *29*, 15-21. 10.1093/bioinformatics/bts635.
Ducceschi, M., Clifton, L.G., Stimpson, S.A., and Billin, A.N. (2014). Post-transcriptional regulation of ITGB6 protein levels in damaged skeletal muscle. J. Mol. Histol. *45*, 329-336. 10.1007/s10735-014-9567-2.
Edelblum, K.L., Shen, L., Weber, C.R., Marchiando, A.M., Clay, B.S., Wang, Y., Prinz, I., Malissen, B., Sperling, A.I., and Turner, J.R. (2012). Dynamic migration of gammadelta intraepithelial lymphocytes requires occludin. Proc. Natl. Acad. Sci. U. S. A. *109*, 7097-7102. 10.1073/pnas.1112519109.
Edele, F., Molenaar, R., Gutle, D., Dudda, J.C., Jakob, T., Homey, B., Mebius, R., Hornef, M., and Martin, S.F. (2008). Cutting edge: instructive role of peripheral tissue cells in the imprinting of T cell homing receptor patterns. J. Immunol. *181*, 3745-3749.
Francis, S.A., Shen, X., Young, J.B., Kaul, P., and Lerner, D.J. (2006). Rho GEF Lsc is required for normal polarization, migration, and adhesion of formyl-peptide-stimulated neutrophils. Blood *107*, 1627-1635. 2005-03-1164 [pii]

10.1182/blood-2005-03-1164.
Frasch, S.C., McNamee, E.N., Kominsky, D., Jedlicka, P., Jakubzick, C., Zemski Berry, K., Mack, M., Furuta, G.T., Lee, J.J., Henson, P.M., et al. (2016). G2A Signaling Dampens Colitic Inflammation via Production of IFN-gamma. J. Immunol. *197*, 1425-1434. 10.4049/jimmunol.1600264.
Green, J.A., and Cyster, J.G. (2012). S1PR2 links germinal center confinement and growth regulation. Immunol. Rev. *247*, 36-51. 10.1111/j.1600-065X.2012.01114.x.
Habtezion, A., Nguyen, L.P., Hadeiba, H., and Butcher, E.C. (2016). Leukocyte Trafficking to the Small Intestine and Colon. Gastroenterology *150*, 340-354. 10.1053/j.gastro.2015.10.046.
Hammerschmidt, S.I., Ahrendt, M., Bode, U., Wahl, B., Kremmer, E., Forster, R., and Pabst, O. (2008). Stromal mesenteric lymph node cells are essential for the generation of gut-homing T cells in vivo. J. Exp. Med. *205*, 2483-2490. jem.20080039 [pii]

10.1084/jem.20080039.
Hao, Y., Hao, S., Andersen-Nissen, E., Mauck, W.M., 3rd, Zheng, S., Butler, A., Lee, M.J., Wilk, A.J., Darby, C., Zager, M., et al. (2021). Integrated analysis of multimodal single-cell data. Cell *184*, 3573-3587 e3529. 10.1016/j.cell.2021.04.048.
Hara, T., Shitara, S., Imai, K., Miyachi, H., Kitano, S., Yao, H., Tani-ichi, S., and Ikuta, K. (2012). Identification of IL-7-producing cells in primary and secondary lymphoid organs using IL-7-GFP knock-in mice. J. Immunol. *189*, 1577-1584. 10.4049/jimmunol.1200586.
Hoytema van Konijnenburg, D.P., Reis, B.S., Pedicord, V.A., Farache, J., Victora, G.D., and Mucida, D. (2017). Intestinal Epithelial and Intraepithelial T Cell Crosstalk Mediates a Dynamic Response to Infection. Cell *171*, 783-794 e713. 10.1016/j.cell.2017.08.046.
Hu, M.D., Ethridge, A.D., Lipstein, R., Kumar, S., Wang, Y., Jabri, B., Turner, J.R., and Edelblum, K.L. (2018). Epithelial IL-15 Is a Critical Regulator of gammadelta Intraepithelial Lymphocyte Motility within the Intestinal Mucosa. J. Immunol. *201*, 747-756. 10.4049/jimmunol.1701603.
Hu, Y., Hu, Q., Li, Y., Lu, L., Xiang, Z., Yin, Z., Kabelitz, D., and Wu, Y. (2023). gammadelta T cells: origin and fate, subsets, diseases and immunotherapy. Signal Transduct Target Ther *8*, 434. 10.1038/s41392-023-01653-8.

Huang, W., Morales, J.L., Gazivoda, V.P., Lai, J., Qi, Q., and August, A. (2013). The zinc-binding region of IL-2 inducible T cell kinase (Itk) is required for interaction with Galpha13 and activation of serum response factor. Int. J. Biochem. Cell Biol. *45*, 1074-1082. 10.1016/j.biocel.2013.02.011.
Jackson, D.P., Joshi, A.D., and Elferink, C.J. (2015). Ah Receptor Pathway Intricacies; Signaling Through Diverse Protein Partners and DNA-Motifs. Toxicol Res (Camb) *4*, 1143-1158. 10.1039/c4tx00236a.
James, O.J., Vandereyken, M., Marchingo, J.M., Singh, F., Bray, S.E., Wilson, J., Love, A.G., and Swamy, M. (2021). IL-15 and PIM kinases direct the metabolic programming of intestinal intraepithelial lymphocytes. Nature communications *12*, 4290. 10.1038/s41467-021-24473-2.
Jarjour, N.N., Dalzell, T.S., Maurice, N.J., Wanhainen, K.M., Peng, C., O'Flanagan, S.D., DePauw, T.A., Block, K.E., Valente, W.J., Ashby, K.M., et al. (2025). Collaboration between interleukin-7 and -15 enables adaptation of tissue-resident and circulating memory CD8(+) T cells to cytokine deficiency. Immunity *58*, 616-631 e615. 10.1016/j.immuni.2025.02.009.
Johansson-Lindbom, B., and Agace, W.W. (2007). Generation of gut-homing T cells and their localization to the small intestinal mucosa. Immunol. Rev. *215*, 226-242. 10.1111/j.1600-065X.2006.00482.x.
Kabarowski, J.H., Zhu, K., Le, L.Q., Witte, O.N., and Xu, Y. (2001). Lysophosphatidylcholine as a ligand for the immunoregulatory receptor G2A. Science *293*, 702-705. 10.1126/science.1061781.
Kennedy, M.K., Glaccum, M., Brown, S.N., Butz, E.A., Viney, J.L., Embers, M., Matsuki, N., Charrier, K., Sedger, L., Willis, C.R., et al. (2000). Reversible defects in natural killer and memory CD8 T cell lineages in interleukin 15-deficient mice. J. Exp. Med. *191*, 771-780. 10.1084/jem.191.5.771.
Konjar, S., Frising, U.C., Ferreira, C., Hinterleitner, R., Mayassi, T., Zhang, Q., Blankenhaus, B., Haberman, N., Loo, Y., Guedes, J., et al. (2018). Mitochondria maintain controlled activation state of epithelial-resident T lymphocytes. Sci Immunol *3*. 10.1126/sciimmunol.aan2543.
Konkel, J.E., Maruyama, T., Carpenter, A.C., Xiong, Y., Zamarron, B.F., Hall, B.E., Kulkarni, A.B., Zhang, P., Bosselut, R., and Chen, W. (2011). Control of the development of CD8alphaalpha+ intestinal intraepithelial lymphocytes by TGF-beta. Nat. Immunol. *12*, 312-319. 10.1038/ni.1997.
Kuen, D.S., Park, M., Ryu, H., Choi, G., Moon, Y.H., Kim, J.O., Kang, K.W., Kim, S.G., and Chung, Y. (2021). Critical regulation of follicular helper T cell differentiation and function by Galpha(13) signaling. Proc. Natl. Acad. Sci. U. S. A. *118*. 10.1073/pnas.2108376118.
Kumar, A., Kremer, K.N., Dominguez, D., Tadi, M., and Hedin, K.E. (2011). Galpha13 and Rho mediate endosomal trafficking of CXCR4 into Rab11+ vesicles upon stromal cell-derived factor-1 stimulation. J. Immunol. *186*, 951-958. 10.4049/jimmunol.1002019.
Kurd, N.S., He, Z., Louis, T.L., Milner, J.J., Omilusik, K.D., Jin, W., Tsai, M.S., Widjaja, C.E., Kanbar, J.N., Olvera, J.G., et al. (2020). Early precursors and molecular determinants of tissue-resident memory CD8(+) T lymphocytes revealed by single-cell RNA sequencing. Sci Immunol *5*. 10.1126/sciimmunol.aaz6894.
Lahvic, J.L., Ammerman, M., Li, P., Blair, M.C., Stillman, E.R., Fast, E.M., Robertson, A.L., Christodoulou, C., Perlin, J.R., Yang, S., et al. (2018). Specific oxylipins enhance vertebrate hematopoiesis via the receptor GPR132. Proc. Natl. Acad. Sci. U. S. A. *115*, 9252-9257. 10.1073/pnas.1806077115.
Laidlaw, B.J., Gray, E.E., Zhang, Y., Ramirez-Valle, F., and Cyster, J.G. (2019). Sphingosine-1-phosphate receptor 2 restrains egress of gammadelta T cells from the skin. J. Exp. Med. *216*, 1487-1496. 10.1084/jem.20190114.
Le, L.Q., Kabarowski, J.H., Weng, Z., Satterthwaite, A.B., Harvill, E.T., Jensen, E.R., Miller, J.F., and Witte, O.N. (2001). Mice lacking the orphan G protein-coupled receptor G2A develop a late-onset autoimmune syndrome. Immunity *14*, 561-571. 10.1016/s1074-7613(01)00145-5.

Li, B., and Dewey, C.N. (2011). RSEM: accurate transcript quantification from RNA-Seq data with or without a reference genome. BMC bioinformatics *12*, 323. 10.1186/1471-2105-12-323.
Li, Y., Innocentin, S., Withers, D.R., Roberts, N.A., Gallagher, A.R., Grigorieva, E.F., Wilhelm, C., and Veldhoen, M. (2011). Exogenous stimuli maintain intraepithelial lymphocytes via aryl hydrocarbon receptor activation. Cell *147*, 629-640. 10.1016/j.cell.2011.09.025.
Liu, D., Duan, L., Rodda, L.B., Lu, E., Xu, Y., An, J., Qiu, L., Liu, F., Looney, M.R., Yang, Z., et al. (2022). CD97 promotes spleen dendritic cell positioning and homeostasis through sensing of red blood cells. Science *375*, eabi5965. 10.1126/science.abi5965.
Liu, Q., Chen, P.A., Urs, E., Zhang, S., Arce, M.M., Wang, C.H., Li, Z., Seo, J., Kale, N., LaFlam, T.N., et al. (2025). In vivo genome-wide CRISPR screens in human T cells to enhance T cell therapy for solid tumors. bioRxiv. 10.1101/2025.09.23.678127.
Lodolce, J.P., Boone, D.L., Chai, S., Swain, R.E., Dassopoulos, T., Trettin, S., and Ma, A. (1998). IL-15 receptor maintains lymphoid homeostasis by supporting lymphocyte homing and proliferation. Immunity *9*, 669-676.
Love, M.I., Huber, W., and Anders, S. (2014). Moderated estimation of fold change and dispersion for RNA-seq data with DESeq2. Genome Biol. *15*, 550. 10.1186/s13059-014-0550-8.
Lu, E., and Cyster, J.G. (2019). G-protein coupled receptors and ligands that organize humoral immune responses. Immunol. Rev. *289*, 158-172. 10.1111/imr.12743.
Matloubian, M., Lo, C.G., Cinamon, G., Lesneski, M.J., Xu, Y., Brinkmann, V., Allende, M.L., Proia, R.L., and Cyster, J.G. (2004). Lymphocyte egress from thymus and peripheral lymphoid organs is dependent on S1P receptor 1. Nature *427*, 355-360.
McDonald, B.D., Jabri, B., and Bendelac, A. (2018). Diverse developmental pathways of intestinal intraepithelial lymphocytes. Nat. Rev. Immunol. *18*, 514-525. 10.1038/s41577-018-0013-7.
Meehan, T.F., Witherden, D.A., Kim, C.H., Sendaydiego, K., Ye, I., Garijo, O., Komori, H.K., Kumanogoh, A., Kikutani, H., Eckmann, L., and Havran, W.L. (2014). Protection against colitis by CD100-dependent modulation of intraepithelial gammadelta T lymphocyte function. Mucosal Immunol *7*, 134-142. 10.1038/mi.2013.32.
Mohammed, J., Beura, L.K., Bobr, A., Astry, B., Chicoine, B., Kashem, S.W., Welty, N.E., Igyarto, B.Z., Wijeyesinghe, S., Thompson, E.A., et al. (2016). Stromal cells control the epithelial residence of DCs and memory T cells by regulated activation of TGF-beta. Nat. Immunol. *17*, 414-421. 10.1038/ni.3396.
Molenaar, R., Greuter, M., van der Marel, A.P., Roozendaal, R., Martin, S.F., Edele, F., Huehn, J., Forster, R., O'Toole, T., Jansen, W., et al. (2009). Lymph node stromal cells support dendritic cell-induced gut-homing of T cells. J. Immunol. *183*, 6395-6402. 10.4049/jimmunol.0900311.
Mortier, E., Advincula, R., Kim, L., Chmura, S., Barrera, J., Reizis, B., Malynn, B.A., and Ma, A. (2009). Macrophage- and dendritic-cell-derived interleukin-15 receptor alpha supports homeostasis of distinct CD8+ T cell subsets. Immunity *31*, 811-822. 10.1016/j.immuni.2009.09.017.
Muppidi, J.R., Lu, E., and Cyster, J.G. (2015). The G protein-coupled receptor P2RY8 and follicular dendritic cells promote germinal center confinement of B cells, whereas S1PR3 can contribute to their dissemination. J. Exp. Med. *212*, 2213-2222. 10.1084/jem.20151250.
Muppidi, J.R., Schmitz, R., Green, J.A., Xiao, W., Larsen, A.B., Braun, S.E., An, J., Xu, Y., Rosenwald, A., Ott, G., et al. (2014). Loss of signalling via Galpha13 in germinal centre B-cell-derived lymphoma. Nature *516*, 254-258. 10.1038/nature13765.
Nakajima, H., Nakajima, H.O., Salcher, O., Dittie, A.S., Dembowsky, K., Jing, S., and Field, L.J. (2000). Atrial but not ventricular fibrosis in mice expressing a mutant transforming growth factor-beta(1) transgene in the heart. Circ. Res. *86*, 571-579. 10.1161/01.res.86.5.571.
Nakata, A., Urano, D., Fujii-Kuriyama, Y., Mizuno, N., Tago, K., and Itoh, H. (2009). G-protein signalling negatively regulates the stability of aryl hydrocarbon receptor. EMBO Rep. *10*, 622-628. 10.1038/embor.2009.35.

Nakazato, K., Yamada, H., Yajima, T., Kagimoto, Y., Kuwano, H., and Yoshikai, Y. (2007). Enforced expression of Bcl-2 partially restores cell numbers but not functions of TCRgammadelta intestinal intraepithelial T lymphocytes in IL-15-deficient mice. J. Immunol. *178*, 757-764. 10.4049/jimmunol.178.2.757.
Nguyen, H.T., Li, M., Vadakath, R., Henke, K.A., Tran, T.C., Li, H., Yamadi, M., Darbha, S., Yang, Y., Kabat, J., et al. (2024). Galpha13 restricts nutrient driven proliferation in mucosal germinal centers. Nat. Immunol. *25*, 1718-1730. 10.1038/s41590-024-01910-0.
Obinata, H., Hattori, T., Nakane, S., Tatei, K., and Izumi, T. (2005). Identification of 9-hydroxyoctadecadienoic acid and other oxidized free fatty acids as ligands of the G protein-coupled receptor G2A. J. Biol. Chem. *280*, 40676-40683. 10.1074/jbc.M507787200.
Okada, T., and Cyster, J.G. (2007). CC Chemokine Receptor 7 Contributes to Gi-Dependent T Cell Motility in the Lymph Node. J. Immunol. *178*, 2973-2978.
Qiu, Z., Khairallah, C., Chu, T.H., Imperato, J.N., Lei, X., Romanov, G., Atakilit, A., Puddington, L., and Sheridan, B.S. (2023). Retinoic acid signaling during priming licenses intestinal CD103+ CD8 TRM cell differentiation. J. Exp. Med. *220*. 10.1084/jem.20210923.
Radu, C.G., Yang, L.V., Riedinger, M., Au, M., and Witte, O.N. (2004). T cell chemotaxis to lysophosphatidylcholine through the G2A receptor. Proc. Natl. Acad. Sci. U. S. A. *101*, 245-250. 10.1073/pnas.2536801100.
Rathmell, J.C., Farkash, E.A., Gao, W., and Thompson, C.B. (2001). IL-7 enhances the survival and maintains the size of naive T cells. J. Immunol. *167*, 6869-6876. 10.4049/jimmunol.167.12.6869.
Reina-Campos, M., Monell, A., Ferry, A., Luna, V., Cheung, K.P., Galletti, G., Scharping, N.E., Takehara, K.K., Quon, S., Challita, P.P., et al. (2025). Tissue-resident memory CD8 T cell diversity is spatiotemporally imprinted. Nature *639*, 483-492. 10.1038/s41586-024-08466-x.
Richon, S., Zajac, O., Perez Gonzalez, C., and Matic Vignjevic, D. (2023). Optimized protocol for the generation of an orthotopic colon cancer mouse model and metastasis. STAR Protoc *4*, 102022. 10.1016/j.xpro.2022.102022.
Rubtsov, A., Strauch, P., Digiacomo, A., Hu, J., Pelanda, R., and Torres, R.M. (2005). Lsc regulates marginal-zone B cell migration and adhesion and is required for the IgM T-dependent antibody response. Immunity *23*, 527-538.
Ruppel, K.M., Willison, D., Kataoka, H., Wang, A., Zheng, Y.W., Cornelissen, I., Yin, L., Xu, S.M., and Coughlin, S.R. (2005). Essential role for Galpha13 in endothelial cells during embryonic development. Proc. Natl. Acad. Sci. U. S. A. *102*, 8281-8286. 0503326102 [pii]

10.1073/pnas.0503326102.
Schluns, K.S., Nowak, E.C., Cabrera-Hernandez, A., Puddington, L., Lefrancois, L., and Aguila, H.L. (2004). Distinct cell types control lymphoid subset development by means of IL-15 and IL-15 receptor alpha expression. Proc. Natl. Acad. Sci. U. S. A. *101*, 5616-5621. 10.1073/pnas.0307442101.
Shalapour, S., Deiser, K., Sercan, O., Tuckermann, J., Minnich, K., Willimsky, G., Blankenstein, T., Hammerling, G.J., Arnold, B., and Schuler, T. (2010). Commensal microflora and interferon-gamma promote steady-state interleukin-7 production in vivo. Eur. J. Immunol. *40*, 2391-2400. 10.1002/eji.201040441.
Sheridan, B.S., Pham, Q.M., Lee, Y.T., Cauley, L.S., Puddington, L., and Lefrancois, L. (2014). Oral infection drives a distinct population of intestinal resident memory CD8(+) T cells with enhanced protective function. Immunity *40*, 747-757. 10.1016/j.immuni.2014.03.007.
Siehler, S. (2009). Regulation of RhoGEF proteins by G12/13-coupled receptors. Br. J. Pharmacol. *158*, 41-49. BPH121 [pii]

10.1111/j.1476-5381.2009.00121.x.

Sumida, H., Lu, E., Chen, H., Yang, Q., Mackie, K., and Cyster, J.G. (2017). GPR55 regulates intraepithelial lymphocyte migration dynamics and susceptibility to intestinal damage. Sci Immunol *2*, eaao1135. 10.1126/sciimmunol.aao1135.
Sun, X., Cai, Y., Fleming, C., Tong, Z., Wang, Z., Ding, C., Qu, M., Zhang, H.G., Suo, J., and Yan, J. (2017). Innate gammadeltaT17 cells play a protective role in DSS-induced colitis via recruitment of Gr-1(+)CD11b(+) myeloid suppressor cells. Oncoimmunology *6*, e1313369. 10.1080/2162402X.2017.1313369.
Svensson, M., Johansson-Lindbom, B., Zapata, F., Jaensson, E., Austenaa, L.M., Blomhoff, R., and Agace, W.W. (2008). Retinoic acid receptor signaling levels and antigen dose regulate gut homing receptor expression on CD8+ T cells. Mucosal Immunol *1*, 38-48. 10.1038/mi.2007.4.
Takei, Y., Nemoto, Y., Morikawa, R., Tanaka, S., Oshima, S., Nagaishi, T., Okamoto, R., Tsuchiya, K., Nakamura, T., and Watanabe, M. (2020). CD8alphaalpha(+) T cells show amoeboid shape and frequent morphological change in vitro, and localize to small intestinal intraepithelial region in vivo. Biochem. Biophys. Res. Commun. *523*, 328-335. 10.1016/j.bbrc.2019.12.021.
Takuwa, N., Du, W., Kaneko, E., Okamoto, Y., Yoshioka, K., and Takuwa, Y. (2011). Tumor-suppressive sphingosine-1-phosphate receptor-2 counteracting tumor-promoting sphingosine-1-phosphate receptor-1 and sphingosine kinase 1 - Jekyll Hidden behind Hyde. American journal of cancer research *1*, 460-481.
Thompson, E.A., Mitchell, J.S., Beura, L.K., Torres, D.J., Mrass, P., Pierson, M.J., Cannon, J.L., Masopust, D., Fife, B.T., and Vezys, V. (2019). Interstitial Migration of CD8alphabeta T Cells in the Small Intestine Is Dynamic and Is Dictated by Environmental Cues. Cell Rep *26*, 2859-2867 e2854. 10.1016/j.celrep.2019.02.034.
Tsuchiya, T., Fukuda, S., Hamada, H., Nakamura, A., Kohama, Y., Ishikawa, H., Tsujikawa, K., and Yamamoto, H. (2003). Role of gamma delta T cells in the inflammatory response of experimental colitis mice. J. Immunol. *171*, 5507-5513. 10.4049/jimmunol.171.10.5507.
Wang, J.L., Dou, X.D., Cheng, J., Gao, M.X., Xu, G.F., Ding, W., Ding, J.H., Li, Y., Wang, S.H., Ji, Z.W., et al. (2023). Functional screening and rational design of compounds targeting GPR132 to treat diabetes. Nat Metab *5*, 1726-1746. 10.1038/s42255-023-00899-4.
Wang, L., Radu, C.G., Yang, L.V., Bentolila, L.A., Riedinger, M., and Witte, O.N. (2005). Lysophosphatidylcholine-induced surface redistribution regulates signaling of the murine G protein-coupled receptor G2A. Mol. Biol. Cell *16*, 2234-2247. 10.1091/mbc.e04-12-1044.
Watanabe, M., Ueno, Y., Yajima, T., Okamoto, S., Hayashi, T., Yamazaki, M., Iwao, Y., Ishii, H., Habu, S., Uehira, M., et al. (1998). Interleukin 7 transgenic mice develop chronic colitis with decreased interleukin 7 protein accumulation in the colonic mucosa. J. Exp. Med. *187*, 389-402. 10.1084/jem.187.3.389.
Xing, Q., Chang, D., Xie, S., Zhao, X., Zhang, H., Wang, X., Bai, X., and Dong, C. (2024). BCL6 is required for the thymic development of TCRalphabeta(+)CD8alphaalpha(+) intraepithelial lymphocyte lineage. Sci Immunol *9*, eadk4348. 10.1126/sciimmunol.adk4348.
Xu, J., Wang, F., Van Keymeulen, A., Herzmark, P., Straight, A., Kelly, K., Takuwa, Y., Sugimoto, N., Mitchison, T., and Bourne, H.R. (2003). Divergent signals and cytoskeletal assemblies regulate self-organizing polarity in neutrophils. Cell *114*, 201-214.
Yagi, H., Tan, W., Dillenburg-Pilla, P., Armando, S., Amornphimoltham, P., Simaan, M., Weigert, R., Molinolo, A.A., Bouvier, M., and Gutkind, J.S. (2011). A synthetic biology approach reveals a CXCR4-G13-Rho signaling axis driving transendothelial migration of metastatic breast cancer cells. Sci Signal *4*, ra60. 10.1126/scisignal.2002221.
Yang, L.V., Radu, C.G., Wang, L., Riedinger, M., and Witte, O.N. (2005). Gi-independent macrophage chemotaxis to lysophosphatidylcholine via the immunoregulatory GPCR G2A. Blood *105*, 1127-1134. 10.1182/blood-2004-05-1916.
Yang, Y.M., Kuen, D.-S., CHung, Y., Kurose, H., and Kim, S.G. (2020). Gα12/13 signaling in metabolic diseases. Experimental & Molecular Medicine *52*, 896-910.

Zhang, B., Wu, J., Jiao, Y., Bock, C., Dai, M., Chen, B., Chao, N., Zhang, W., and Zhuang, Y. (2015). Differential Requirements of TCR Signaling in Homeostatic Maintenance and Function of Dendritic Epidermal T Cells. J. Immunol. *195*, 4282-4291. 10.4049/jimmunol.1501220.
Zhang, N., and Bevan, M.J. (2013). Transforming growth factor-beta signaling controls the formation and maintenance of gut-resident memory T cells by regulating migration and retention. Immunity *39*, 687-696. 10.1016/j.immuni.2013.08.019.
Zhao, X., Li, L., Starr, T.K., and Subramanian, S. (2017). Tumor location impacts immune response in mouse models of colon cancer. Oncotarget *8*, 54775-54787. 10.18632/oncotarget.18423.
Zheng, G.X., Terry, J.M., Belgrader, P., Ryvkin, P., Bent, Z.W., Wilson, R., Ziraldo, S.B., Wheeler, T.D., McDermott, G.P., Zhu, J., et al. (2017). Massively parallel digital transcriptional profiling of single cells. Nature communications *8*, 14049. 10.1038/ncomms14049.
Zigmond, E., Halpern, Z., Elinav, E., Brazowski, E., Jung, S., and Varol, C. (2011). Utilization of murine colonoscopy for orthotopic implantation of colorectal cancer. PLoS One *6*, e28858. 10.1371/journal.pone.0028858.

Figure 1.

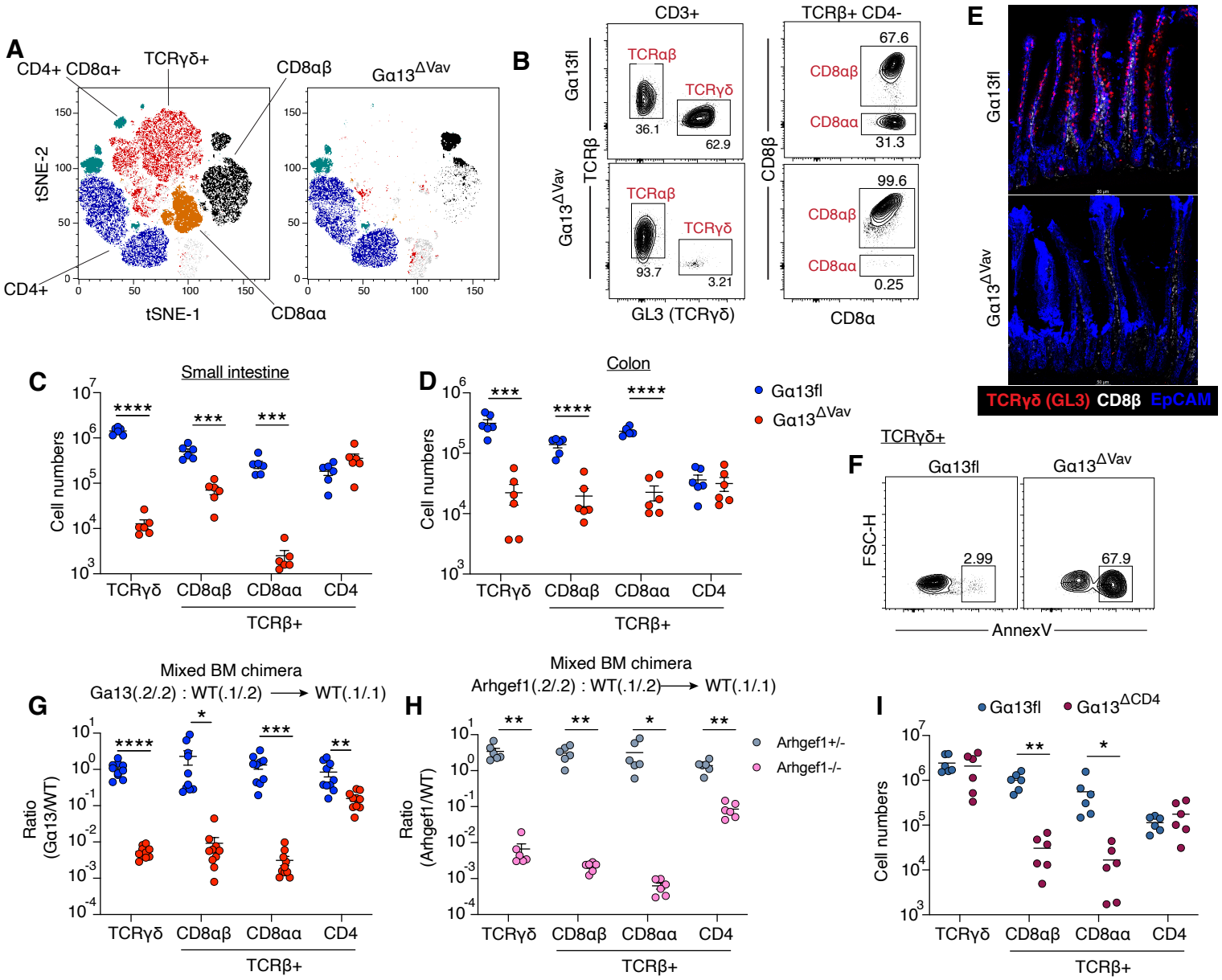
A
CD4+ CD8α+
TCRγδ+
CD8αβ
Gα13ΔVav
tSNE-2
tSNE-1
CD4+
CD8αα
B
CD3+
TCRβ+ CD4-
Gα13fl
Gα13ΔVav
TCRβ
TCRαβ
TCRγδ
36.1
62.9
93.7
3.21
CD8β
CD8αβ
CD8αα
67.6
31.3
99.6
0.25
GL3 (TCRγδ)
CD8α
E
Gα13fl
Gα13ΔVav
TCRγδ (GL3) CD8β EpCAM
C
Small intestine
Cell numbers
TCRγδ
CD8αβ
CD8αα
CD4
TCRβ+
D
Colon
Gα13fl
Gα13ΔVav
TCRγδ+
F
Gα13fl
Gα13ΔVav
FSC-H
2.99
67.9
AnnexV
G
Mixed BM chimera
Ga13(.2/.2) : WT(.1/.2) → WT(.1/.1)
Ratio (Gα13/WT)
H
Mixed BM chimera
Arhgef1(.2/.2) : WT(.1/.2) → WT(.1/.1)
Arhgef1+/-
Arhgef1-/-
Ratio (Arhgef1/WT)
I
Gα13fl
Gα13ΔCD4

Figure 2.

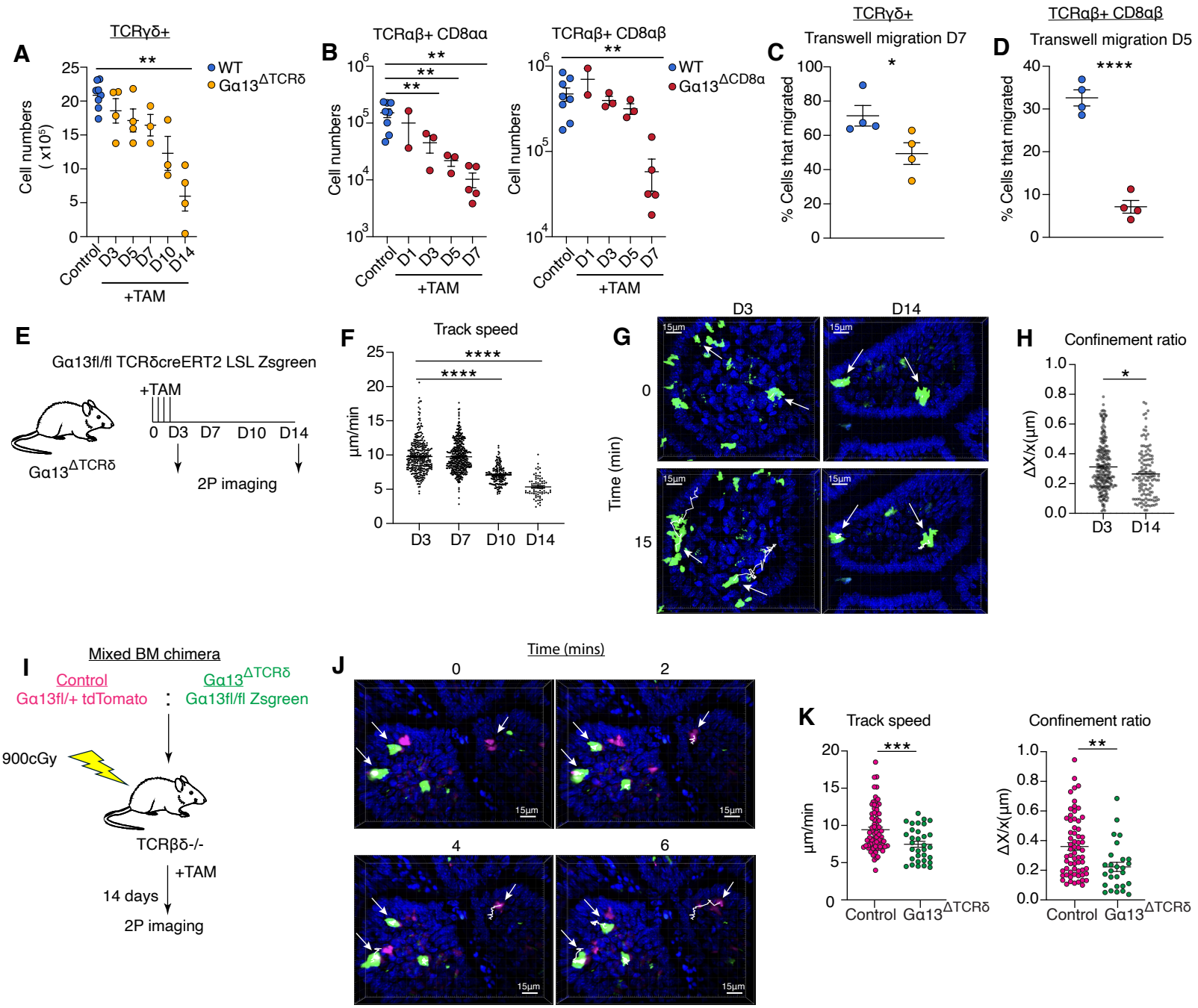
A
TCRγδ+
Cell numbers (x10^5)
WT
Gα13^ΔTCRδ
Control D3 D5 D7 D10 D14
+TAM
B
TCRαβ+ CD8αα
TCRαβ+ CD8αβ
Cell numbers
WT
Gα13^ΔCD8α
Control D1 D3 D5 D7
+TAM
C
TCRγδ+
Transwell migration D7
% Cells that migrated
D
TCRαβ+ CD8αβ
Transwell migration D5
% Cells that migrated
E
Gα13fl/fl TCRδcreERT2 LSL Zsgreen
+TAM
0 D3 D7 D10 D14
Gα13^ΔTCRδ
2P imaging
F
Track speed
μm/min
D3 D7 D10 D14
G
D3
D14
Time (min)
0
15
15μm
H
Confinement ratio
ΔX/x(μm)
D3 D14
I
Mixed BM chimera
Control
Gα13fl/+ tdTomato
Gα13^ΔTCRδ
Gα13fl/fl Zsgreen
900cGy
TCRβδ-/-
+TAM
14 days
2P imaging
J
Time (mins)
0
2
4
6
15μm
K
Track speed
μm/min
Control Gα13^ΔTCRδ
Confinement ratio
ΔX/x(μm)
Control Gα13^ΔTCRδ

Figure 3.

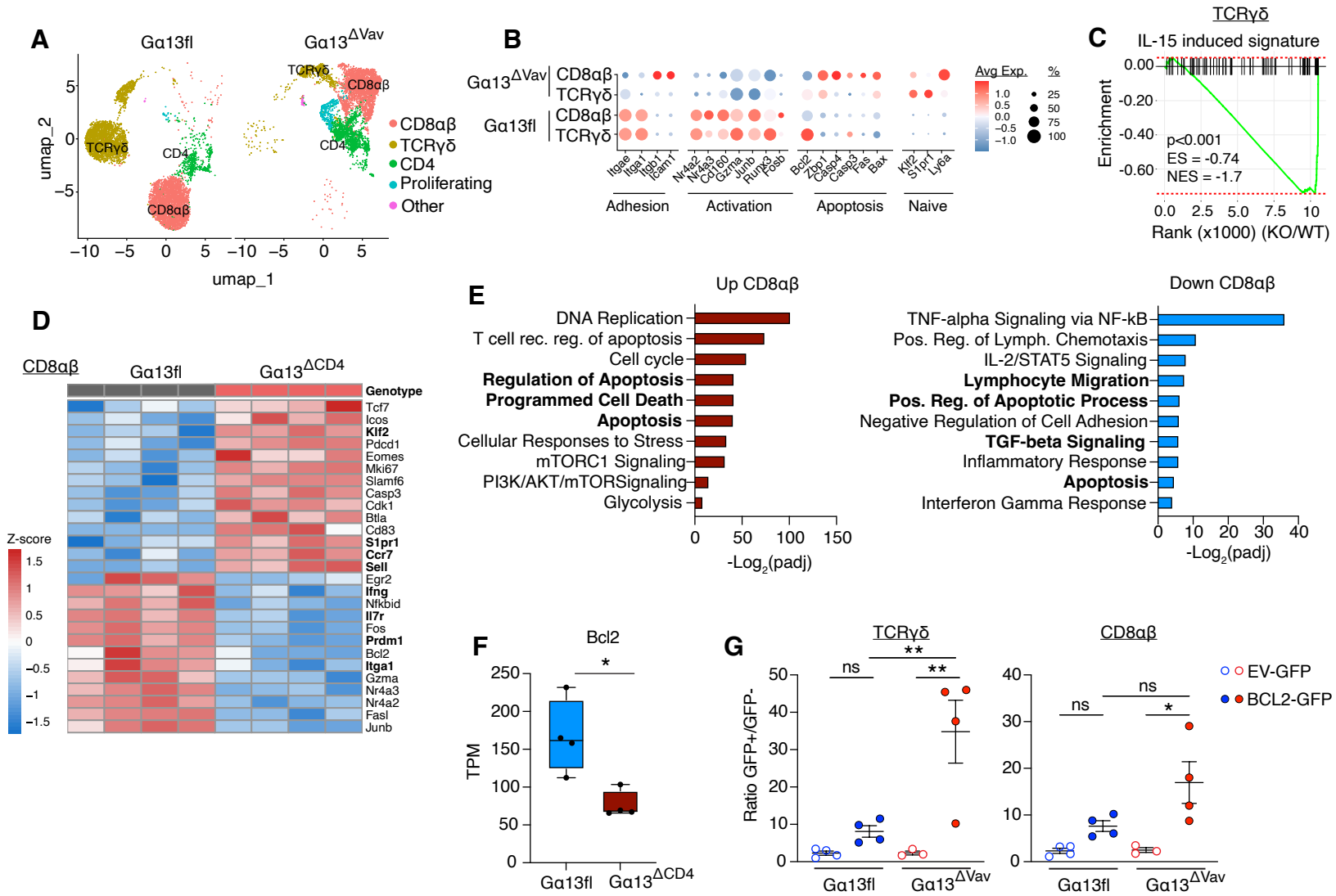
A
Gα13fl
Gα13ΔVav
TCRγδ
CD8αβ
CD4
Proliferating
Other
umap_2
umap_1
B
Gα13ΔVav
Gα13fl
Avg Exp.
%
Adhesion
Activation
Apoptosis
Naive
C
TCRγδ
IL-15 induced signature
Enrichment
p<0.001
ES = -0.74
NES = -1.7
Rank (x1000) (KO/WT)
D
CD8αβ
Gα13fl
Gα13ΔCD4
Genotype
Z-score
E
Up CD8αβ
DNA Replication
T cell rec. reg. of apoptosis
Cell cycle
Regulation of Apoptosis
Programmed Cell Death
Apoptosis
Cellular Responses to Stress
mTORC1 Signaling
PI3K/AKT/mTORSignaling
Glycolysis
-Log2(padj)
Down CD8αβ
TNF-alpha Signaling via NF-kB
Pos. Reg. of Lymph. Chemotaxis
IL-2/STAT5 Signaling
Lymphocyte Migration
Pos. Reg. of Apoptotic Process
Negative Regulation of Cell Adhesion
TGF-beta Signaling
Inflammatory Response
Apoptosis
Interferon Gamma Response
-Log2(padj)
F
Bcl2
TPM
Gα13fl
Gα13ΔCD4
G
TCRγδ
CD8αβ
Ratio GFP+/GFP-
ns
EV-GFP
BCL2-GFP
Gα13fl
Gα13ΔVav

Figure 4.

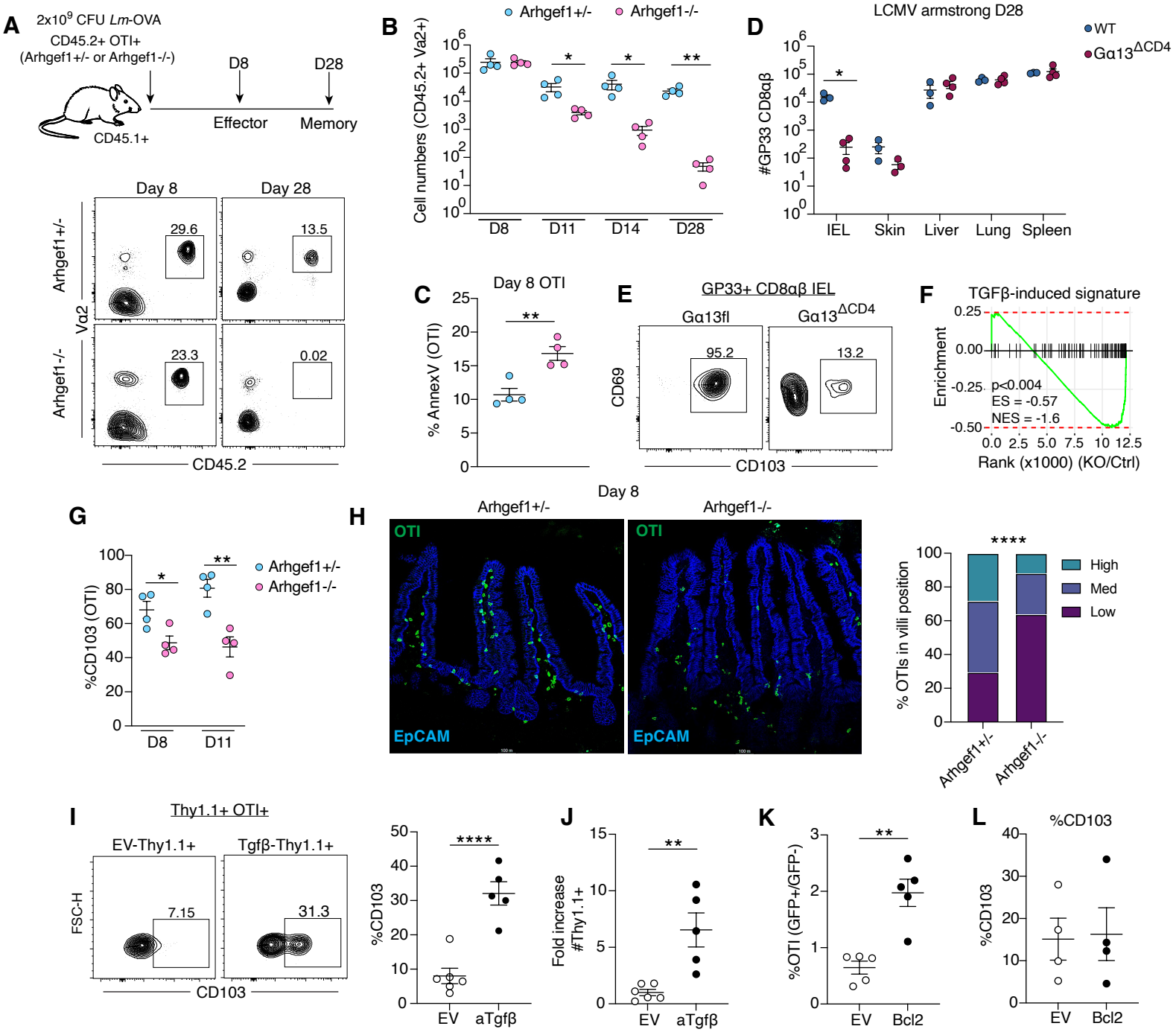
A
2x10^9 CFU Lm-OVA
CD45.2+ OTI+
(Arhgef1+/- or Arhgef1-/-)
D8
D28
Effector
Memory
CD45.1+
Day 8
Day 28
Arhgef1+/-
Arhgef1-/-
Vα2
29.6
13.5
23.3
0.02
CD45.2
B
Arhgef1+/-
Arhgef1-/-
Cell numbers (CD45.2+ Va2+)
D8
D11
D14
D28
C
Day 8 OTI
% AnnexV (OTI)
D
LCMV armstrong D28
WT
Gα13ΔCD4
#GP33 CD8αβ
IEL
Skin
Liver
Lung
Spleen
E
GP33+ CD8αβ IEL
Gα13fl
Gα13ΔCD4
CD69
95.2
13.2
CD103
F
TGFβ-induced signature
Enrichment
p<0.004
ES = -0.57
NES = -1.6
Rank (x1000) (KO/Ctrl)
G
%CD103 (OTI)
Arhgef1+/-
Arhgef1-/-
D8
D11
H
Day 8
Arhgef1+/-
Arhgef1-/-
OTI
EpCAM
% OTIs in villi position
High
Med
Low
I
Thy1.1+ OTI+
EV-Thy1.1+
Tgfβ-Thy1.1+
FSC-H
7.15
31.3
CD103
%CD103
EV
aTgfβ
J
Fold increase #Thy1.1+
K
%OTI (GFP+/GFP-)
Bcl2
L
%CD103

Figure 5.

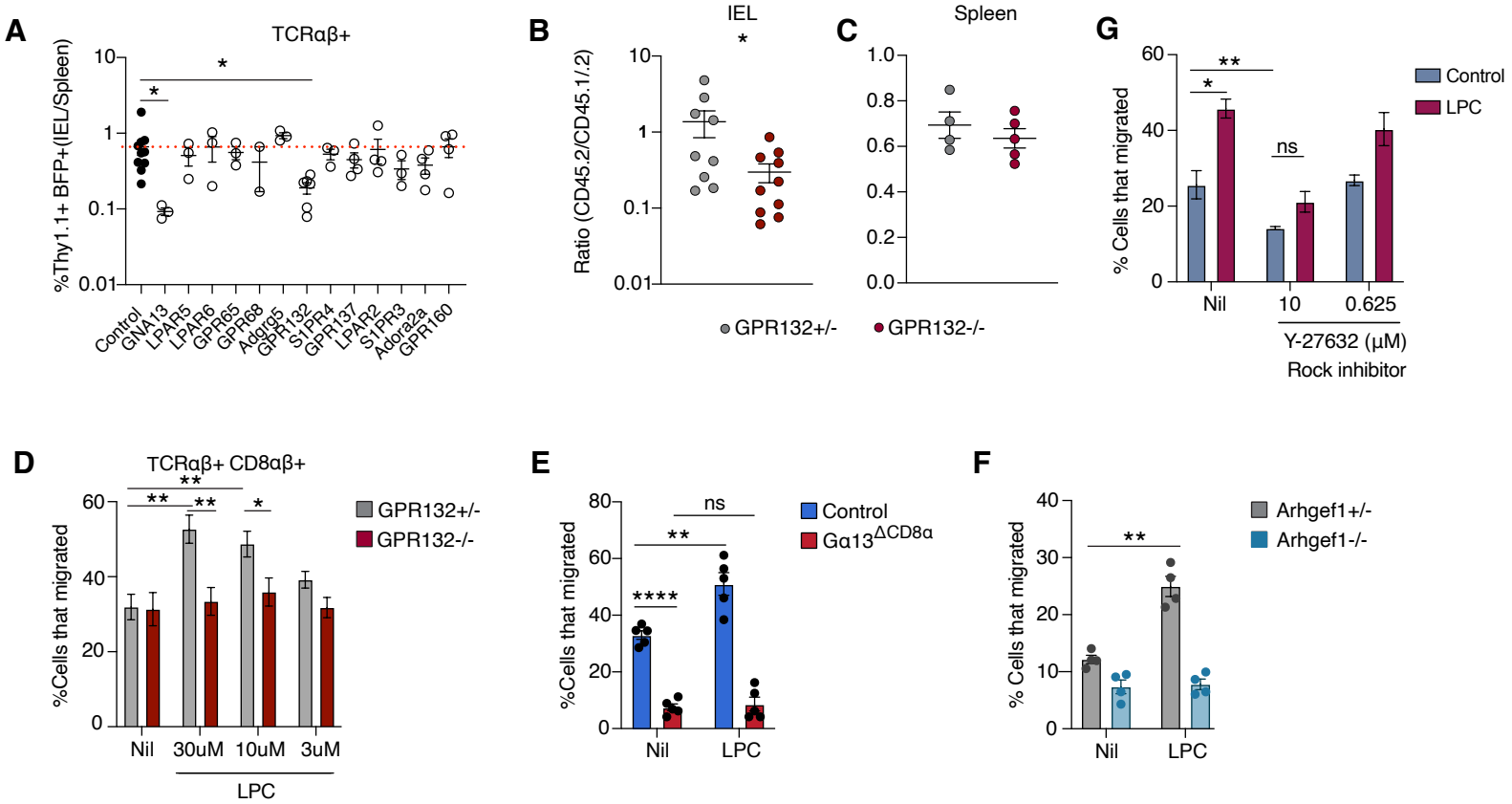
A
TCRαβ+
%Thy1.1+ BFP+(IEL/Spleen)
10
1
0.1
0.01
*
*
Control
GNA13
LPAR5
LPAR6
GPR65
GPR68
Adgrg5
GPR132
S1PR4
GPR137
LPAR2
S1PR3
Adora2a
GPR160
B
IEL
Ratio (CD45.2/CD45.1/2)
10
1
0.1
0.01
*
C
Spleen
1.0
0.8
0.6
0.4
0.2
0.0
GPR132+/-
GPR132-/-
G
% Cells that migrated
60
40
20
0
**
*
ns
Control
LPC
Nil
10
0.625
Y-27632 (μM)
Rock inhibitor
D
TCRαβ+ CD8αβ+
%Cells that migrated
60
40
20
0
**
**
**
*
GPR132+/-
GPR132-/-
Nil
30uM
10uM
3uM
LPC
E
%Cells that migrated
80
60
40
20
0
ns
**
****
Control
Gα13ΔCD8α
Nil
LPC
F
% Cells that migrated
40
30
20
10
0
**
Arhgef1+/-
Arhgef1-/-
Nil
LPC

Figure 6.

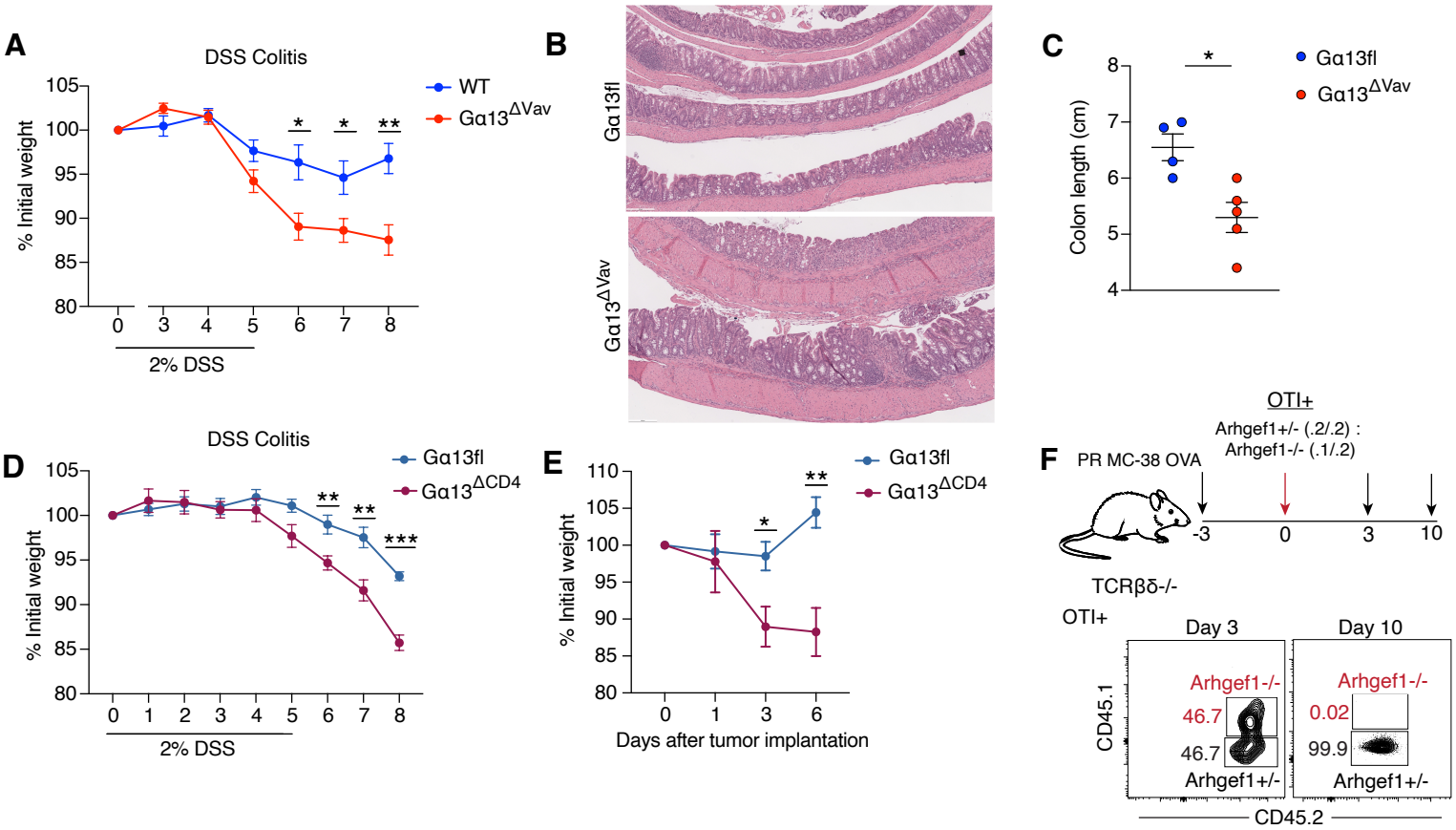
A
DSS Colitis
% Initial weight
WT
Gα13ΔVav
2% DSS
B
Gα13fl
Gα13ΔVav
C
Colon length (cm)
Gα13fl
Gα13ΔVav
D
DSS Colitis
% Initial weight
Gα13fl
Gα13ΔCD4
2% DSS
E
% Initial weight
Gα13fl
Gα13ΔCD4
Days after tumor implantation
F
PR MC-38 OVA
OTI+
Arhgef1+/- (.2/.2) :
Arhgef1-/- (.1/.2)
TCRβδ-/-
OTI+
Day 3
Day 10
Arhgef1-/-
46.7
46.7
Arhgef1+/-
Arhgef1-/-
0.02
99.9
Arhgef1+/-
CD45.1
CD45.2